

Two-dimensional moiré phonon polaritons

Hao Shi,¹ Chu Li,¹ Ding Pan,^{1,2} and Xi Dai¹

¹*Department of Physics, The Hong Kong University of Science and Technology, Clear Water Bay, Hong Kong, China*

²*Department of Chemistry, The Hong Kong University of Science and Technology, Clear Water Bay, Hong Kong, China*

Phonon polaritons are hybrid modes combining lattice dynamics and electromagnetic waves. Their behavior at long wavelengths is effectively described by Huang’s equations. Here, we investigate phonon polaritons within 2D materials featuring twisted moiré structures. The interaction between electromagnetic waves and phonons of varying wavelengths gives rise to rich polaritons with moiré characteristics. We observe the polariton dividing into multiple branches, akin to coupled oscillators. Through numerical simulations based on realistic lattice models, we confirm the existence of these intriguing modes. A distinctive trait of moiré polar crystals is their spatially varying near-field response, offering robust signals for the experimental confirmation.

Introduction. Polaritons arise from the coupling of photons with collective excitations in polar materials, e.g., phonons, plasmons, and excitons. These hybrid modes exhibit properties of both light and matter, allowing for wide applications in fields such as optics [1, 2], condensed matter physics [3, 4], and quantum computing [5, 6]. In polar crystals, ions oscillate with polarization and interact with electromagnetic (EM) waves. The mutual influence between the ionic motion and the EM field gives rise to the phonon polariton (PhP). The first PhP model in 3D crystals traces back to Huang’s equations [7], where the long-wavelength ionic vibration and polarization are treated macroscopically. Solving Huang’s equations combined with Maxwell’s equations gives 3D PhP. Similar macroscopic theory for 2D materials is in place, yet it includes extra constraints arising from the EM boundary conditions [8–16]. The 2D PhP can manifest as either transverse magnetic (TM) or transverse electric (TE) modes, crucially propagating along the material surface. In the out-of-plane direction, the EM fields are localized, forming typical “2D EM waves”.

Moiré superlattices introduce a new potential to engineer 2D physics at length scales much larger than the crystal periodicity, providing a powerful platform for the light-matter interaction [4, 17–19]. Triggered by the discovery of superconducting and correlated insulating states in twisted bilayer graphene [20, 21], emerging exotic phenomena have been discovered in moiré systems [17, 18, 22–34]. Despite the broad interest and progress in this area, the PhP in moiré systems remains poorly explored. This is likely due to the limited resolution of optics, which is beyond the tiny energy scales that typically happen in moiré physics. Moreover, samples under experimental conditions often show larger dissipations, making it challenging to directly detect moiré polaritons. The theoretical challenge stems from the difficulty in accurately handling the huge degree of freedom inherent in moiré superlattices.

Using lattice models, we study PhP in moiré materials, i.e., the twisted bilayer hexagonal boron nitride (hBN) and MoTe₂. In moiré systems, phonons fold into the moiré Brillouin zone (mBZ), forming moiré phonon bands [35, 36]. Each mini band carries some optically

active components by short-ranged elastic hybridization, generating multiple branches of PhPs. These modes are moiré polaritons, whose phonon and EM wave functions show moiré patterns. The resulting local response is typically inhomogeneous [17, 18]. Interestingly, the short-wavelength field components can be excited using an incidence of light with long wavelength. These features never occur in moiré-less materials and 3D crystals. The far-field detection of the dispersion is perhaps challenging due to sample and light source demands. However, thanks to the inhomogeneous property, the near-field techniques offer a more feasible way to capture moiré PhP by enabling scanning across various stacking areas [37].

Theoretical formalism. We start with the 2D PhP formalism. An ionic sheet is placed at $z = 0$ of the vacuum [$\epsilon, \mu = 1$, Fig. 1(a)]. The dynamics is captured by the vibrational field \mathbf{W} satisfying the equation of motion

$$\ddot{\mathbf{W}} = -\omega_0^2 \mathbf{W} + \gamma_{12} \mathbf{E}_t, \quad (1)$$

where ω_0 is the resonance frequency, \mathbf{E}_t is the in-plane part of the electric field \mathbf{E} at $z = 0$. The in-plane polarization density, \mathbf{P} , originates mainly from the ionic displacement:

$$\mathbf{P} = \gamma_{21} \mathbf{W}. \quad (2)$$

The parameters $\gamma_{12} = \gamma_{21} = \sqrt{\epsilon_0 T}$ can be inferred from microscopic models. The above two equations are the 2D versions of Huang’s equations. They should be solved together with Maxwell’s equations and the boundary conditions (BC) at $z = 0$. We study solutions of the form $\mathbf{E}, \mathbf{W} \propto e^{i\mathbf{q}\cdot\mathbf{r} - i\omega t}$, where \mathbf{r} and \mathbf{q} are *in-plane* position and momentum, respectively. The susceptibility can then be defined as

$$\mathbf{P} = \epsilon_0 \Pi(\omega) \mathbf{E}_t, \quad \Pi(\omega) = \frac{T}{\omega_0^2 - \omega^2}. \quad (3)$$

In the non-retarded limit ($c = \infty$), only the electric field is involved. The solutions are divided into transverse (TO) and longitudinal (LO) modes. For the TO mode, pure oscillation $\mathbf{W} \perp \mathbf{q}$ occurs, while $\mathbf{E} = \mathbf{0}$ and the frequency is dispersionless $\omega_{\text{TO}} = \omega_0$. However, the LO

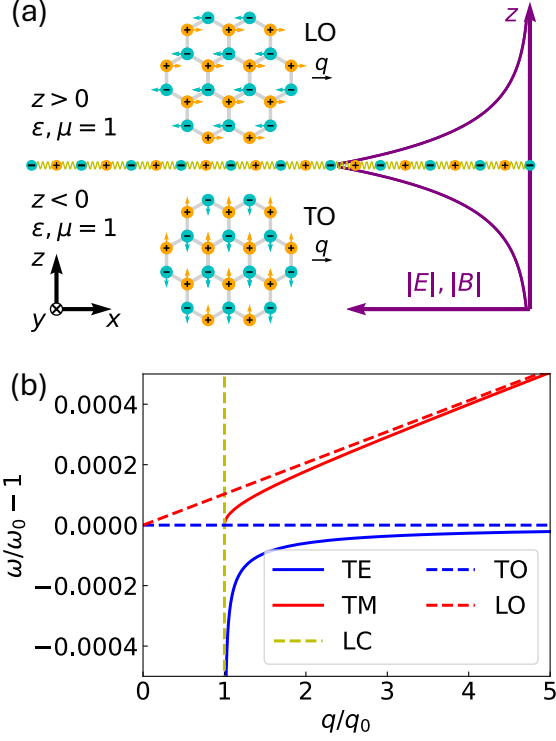


FIG. 1. (a) A 2D polar sheet is placed at $z = 0$ in vacuum. The PhP holds typical 2D EM waves decaying along the z -axis, as sketched by the purple coordinates. The inset shows the long-wavelength ($\mathbf{q} = q\mathbf{e}_x$) LO and TO patterns in the xy -plane for a binary crystal. (b) The 2D PhP dispersion of the TM, TE modes near the light cone (LC) and the resonance frequency ω_0 . For comparison the LO, TO modes with non-retarded approximation are also plotted. In (b) we use $T/(2\omega_0 c) = 2.06 \times 10^{-4}$ obtained from the lattice model of monolayer hBN (see SI).

mode oscillates with the built-in electric field. The eigen equation $1 + q\Pi(\omega)/2 = 0$ gives the long-wavelength linear dispersion with a gap $\omega_{\text{LO}} \approx \omega_0 + qT/(4\omega_0)$ [10, 11, 13, 15].

Once the retardation effect [38] is considered, the solutions can be either guided or radiative modes [39, 40], depending on whether $\lambda = \sqrt{q^2 - \omega^2/c^2}$ is real or imaginary. Radiative solutions live inside the light cone in the (\mathbf{q}, ω) space, where the problem reduces to the traditional light propagation setup with the polar sheet as a scattering interface. The radiative solution thus exists for general (\mathbf{q}, ω) when $\omega \neq \omega_0$. However, we are more interested in guided modes, which have 2D EM waves localized around $z = 0$. The retardation turns the LO eigen equation into $1 + \lambda\Pi(\omega)/2 = 0$. The corresponding EM field is p -polarized (TM, $\mathbf{B} \perp \mathbf{q}$). When $q \gg \omega_0/c$, the TM dispersion is asymptotic with respect to the static LO dispersion. The retardation also brings corrections to the transverse mode, whose dispersion is now governed by $1 - \Pi(\omega)\omega^2/(2\lambda c^2) = 0$, giving an s -polarized EM field

(TE, $\mathbf{E} \perp \mathbf{q}$). When $q \ll \omega_0/c$, the TE mode resembles light, while for $q \gg \omega_0/c$, it turns into pure lattice oscillations. Notice that the TM (TE) mode exists only if $\Pi(\omega) < 0$ [$\Pi(\omega) > 0$]. The PhP dispersions are summarized in Fig. 1(b). They are typical 2D EM waves with energy constrained in the z -axis. Such modes, accompanied by polarizable collective modes, exist ubiquitously at 2D materials and interfaces of 3D materials. The eigenmode conditions are general to use; e.g., when discussing 2D plasmon polaritons one only needs to replace $\Pi(\omega)$ by its plasmon version. The rule is also true that the sign of $\Pi(\omega)$ governs the TM or TE nature. For example, the interband conductivity provides graphene with a specific region where $\Pi(\omega) < 0$, indicating a unique TE plasmon mode [41, 42] that is missing in traditional 2D electron gas [43].

Both the guided and radiative modes can be uniformly treated from a light reflection and refraction viewpoint [44]. In such method the PhP dispersion $\omega(\mathbf{q})$ appears as the poles of the transmission matrix $T(\mathbf{q}, \omega)$, which is of better numerical convenience. Plotting the spectrum $\mathcal{L}(\mathbf{q}, \omega) = -\text{Im}[\det[T(\mathbf{q}, \omega + i\delta)]]$ (the phonon linewidth δ is tiny) visualizes both the continuous spectrum of radiative solutions and dispersions of guided modes.

Things become more interesting in moiré systems. The supercell can become even mesoscopic with a huge sublattice degree of freedom [37]. The elastic phonon folds into the moiré Brillouin zone (mBZ), forming anfractuous moiré phonons [35, 36]. It is then intriguing to imagine how PhP can nest in such complex systems in the presence of long-ranged EM interaction. For quantitative analysis, we use realistic lattice models that avoid the complex ab initio treatment [45]. The short-ranged interaction among ions is described by the force field, as discussed in the supplementary information (SI); while the long-ranged Coulomb force is incorporated into macroscopic electric fields. The displacement \mathbf{u} of the ion located at $\mathbf{r}_{Ii\alpha}$ (I , i , and α are the supercell, atomic cell, and sublattice indices), satisfies the equation of motion

$$M_\alpha \ddot{\mathbf{u}}(\mathbf{r}_{Ii\alpha}) + \sum_{Jj\beta} \Phi_{i\alpha, j\beta} (\mathbf{L}_I - \mathbf{L}_J) \mathbf{u}(\mathbf{r}_{Jj\beta}) - \sum_{\mathbf{Q}} Z_\alpha e \mathbf{E}_{\bar{\mathbf{q}}+\mathbf{Q}, t} e^{i(\bar{\mathbf{q}}+\mathbf{Q}) \cdot \mathbf{r}_{Ii\alpha} - i\omega t} = 0, \quad (4)$$

where Φ is the force constant [46–54], M_α and Z_α are the ionic mass and charge (in the unit of elementary charge e), respectively. The moiré electric field $\mathbf{E}_t = \sum_{\mathbf{Q}} \mathbf{E}_{\bar{\mathbf{q}}+\mathbf{Q}, t} e^{i(\bar{\mathbf{q}}+\mathbf{Q}) \cdot \mathbf{r} - i\omega t}$ has been inserted, with \mathbf{Q} as moiré reciprocal vectors, and $\bar{\mathbf{q}} \in \text{mBZ}$). The polarization density is defined as [7, 11, 55, 56]

$$\mathbf{P}(\mathbf{r}) = \sum_{Ii\alpha} Z_\alpha e \mathbf{u}(\mathbf{r}_{Ii\alpha}) \delta(\mathbf{r} - \mathbf{r}_{Ii\alpha}). \quad (5)$$

The above two equations are the lattice version of Eqs. (1), (2). In the absence of \mathbf{E}_t , Eq. (4) reduces just to the dynamical equation in the usual non-polar phonon

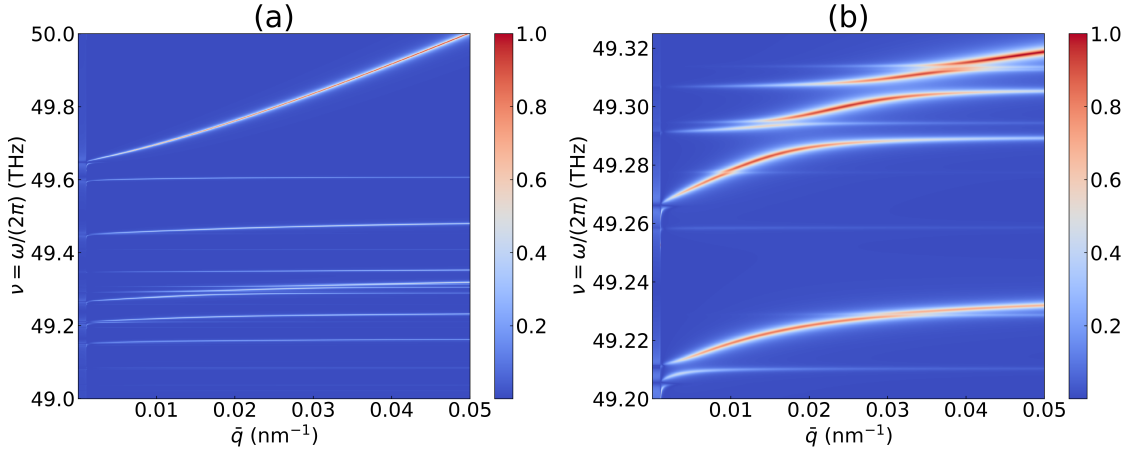


FIG. 2. (a) The long-wavelength PhP dispersion of 2.65° twisted bilayer hBN near $\nu_0 = \omega_0/(2\pi) \approx 49.5$ THz ($q_0 \approx 10^{-3}$ nm^{-1}), along the $\bar{\Gamma} - \bar{M}$ line, obtained by plotting the (normalized) spectrum $\ln(1 + |\mathcal{L}(\bar{q}, \omega + i\delta)|)$. Here a tiny linewidth $\delta/(2\pi) = 10^{-3}$ THz is used to make each branch distinguishable. Many flat branches appear below the topmost dominant branch. (b) The detailed dispersion within the mini window $49.20 \sim 49.325$ THz.

problem. Fortunately, the driven harmonic oscillators can be solved exactly [7]. After some derivation, we find the moiré potential renders the susceptibility into a tensor with multiple poles (see SI). Written in Fourier basis, $\mathbf{P}(\mathbf{r}) = \sum_{\mathbf{Q}} \mathbf{P}_{\bar{\mathbf{q}}+\mathbf{Q}} e^{i(\bar{\mathbf{q}}+\mathbf{Q})\cdot\mathbf{r}-i\omega t}$, we find

$$\begin{aligned} \mathbf{P}_{\bar{\mathbf{q}}+\mathbf{Q}} &= \varepsilon_0 \sum_{\mathbf{Q}'} \mathbf{\Pi}^{\mathbf{Q}\mathbf{Q}'}(\bar{\mathbf{q}}, \omega) \mathbf{E}_{\bar{\mathbf{q}}+\mathbf{Q}', t}, \\ \mathbf{\Pi}^{\mathbf{Q}\mathbf{Q}'}(\bar{\mathbf{q}}, \omega) &= \frac{e^2}{\varepsilon_0 \Omega_m} \sum_b \frac{\mathbf{S}_{Qb}(\bar{\mathbf{q}}) \mathbf{S}_{Q'b}^\dagger(\bar{\mathbf{q}})}{\omega_{qb}^2 - \omega^2}, \end{aligned} \quad (6)$$

where ε_0 is the vacuum permittivity, Ω_m is the supercell area, ω_{qb} and $\mathbf{e}_b(\bar{\mathbf{q}})$ are the bare frequency and displacement vector of the b -th moiré phonon (in the absence of \mathbf{E}_t), and the \mathbf{S} matrix is defined as

$$\mathbf{S}_{Qb}(\bar{\mathbf{q}}) = \sum_{i\alpha} \frac{Z_\alpha \mathbf{e}_{i\alpha, b}(\bar{\mathbf{q}})}{\sqrt{M_\alpha}} e^{-i\mathbf{Q}\cdot(\mathbf{R}_i + \boldsymbol{\tau}_\alpha)}. \quad (7)$$

Moiré physics enter by providing the susceptibility $\mathbf{\Pi}^{\mathbf{Q}\mathbf{Q}'}$ with off-diagonal terms. Notice that $\mathbf{Q} \neq \mathbf{0}$ terms reflect field fluctuations at the moiré length scale [17]. If we turn off the moiré potential, Eq. (6) becomes diagonal about \mathbf{Q} , and $\mathbf{\Pi}^{\mathbf{Q}\mathbf{Q}}$ becomes the moiré-less one (see SI).

The moiré PhP are solved by applying Maxwell's equations and BCs. For simplicity, we assume the moiré material to have zero thickness. After some algebra, the problem reduces to solving $\det[A(\bar{\mathbf{q}}, \omega)] = 0$, where the

matrix elements are

$$\begin{aligned} A_{\parallel\parallel}^{\mathbf{Q}\mathbf{Q}'}(\bar{\mathbf{q}}, \omega) &= \delta_{\mathbf{Q}\mathbf{Q}'} + \frac{\lambda_{\mathbf{Q}}}{2} \mathbf{\Pi}_{\parallel\parallel}^{\mathbf{Q}\mathbf{Q}'}(\bar{\mathbf{q}}, \omega), \\ A_{\parallel\perp}^{\mathbf{Q}\mathbf{Q}'}(\bar{\mathbf{q}}, \omega) &= \frac{\lambda_{\mathbf{Q}}}{2} \mathbf{\Pi}_{\parallel\perp}^{\mathbf{Q}\mathbf{Q}'}(\bar{\mathbf{q}}, \omega), \\ A_{\perp\parallel}^{\mathbf{Q}\mathbf{Q}'}(\bar{\mathbf{q}}, \omega) &= -\frac{1}{2\lambda_{\mathbf{Q}}} \frac{\omega^2}{c^2} \mathbf{\Pi}_{\perp\parallel}^{\mathbf{Q}\mathbf{Q}'}(\bar{\mathbf{q}}, \omega), \\ A_{\perp\perp}^{\mathbf{Q}\mathbf{Q}'}(\bar{\mathbf{q}}, \omega) &= \delta_{\mathbf{Q}\mathbf{Q}'} - \frac{1}{2\lambda_{\mathbf{Q}}} \frac{\omega^2}{c^2} \mathbf{\Pi}_{\perp\perp}^{\mathbf{Q}\mathbf{Q}'}(\bar{\mathbf{q}}, \omega), \end{aligned} \quad (8)$$

written under field components parallel (\parallel) and perpendicular (\perp) to $\bar{\mathbf{q}} + \mathbf{Q}(\mathbf{Q}')$, and $\lambda_{\mathbf{Q}} = \sqrt{|\bar{\mathbf{q}} + \mathbf{Q}|^2 - \omega^2/c^2}$. The above equation is the core result of this paper, which contains all the information about moiré PhP. It is related to the transmission tensor by $T(\bar{\mathbf{q}}, \omega) = A^{-1}(\bar{\mathbf{q}}, \omega)$. The zeros of $\det(A)$ [poles of $\det(T)$] locate the PhP dispersion, whose eigen EM fields read as the corresponding “zero-mode” eigen vectors of A . A salient feature of moiré PhP is that, due to the scattering of moiré potential, a long-wavelength incidence can induce inhomogeneous responses with shorter wavelengths. Based on this property, we can focus on the long-wavelength incidence, which expels those modes with short wavelengths only. The effective transmission matrix is the long-wavelength submatrix $T_{\text{eff}}(\bar{\mathbf{q}}, \omega) = [A^{-1}(\bar{\mathbf{q}}, \omega)]^{\mathbf{00}}$ [18, 31, 57]. The poles of the spectrum $\mathcal{L}(\bar{\mathbf{q}}, \omega) = -\text{Im}[\det[T_{\text{eff}}(\bar{\mathbf{q}}, \omega + i\delta)]]$ depicts the dispersion of moiré PhPs that can be excited by long-wavelength light.

Moiré PhP in hBN and MoTe₂. We choose hBN and MoTe₂ as the playgrounds, which are popular insulating polar crystals [26, 27, 37, 58, 59]. The AA-stacked twisted bilayer structure is adopted.

Hexagonal BN is the traditional polar material in the context of PhP [11–15, 60], with typical optical phonon frequency $\nu_0 = \omega_0/(2\pi) \approx 49.4$ THz. The charge

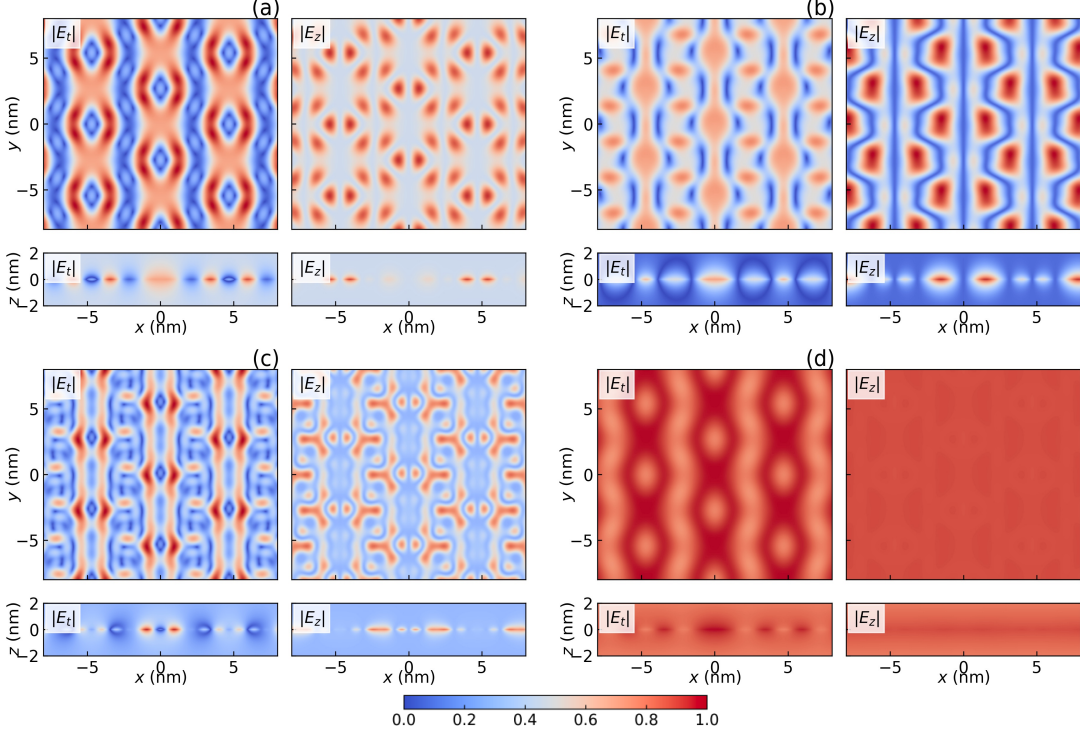


FIG. 3. The in-plane (first row, $z = 0$) and out-of-plane (second row, $y = 0$) distributions of 2.65° twisted bilayer hBN's several eigen fields' amplitudes $|\mathbf{E}_t|$ and $|E_z|$, along the $\bar{\Gamma} - \bar{M}$ line, at (a) $\bar{q} = 0.01 \text{ nm}^{-1}$, $\nu = 49.696 \text{ THz}$, (b) $\bar{q} = 0.01 \text{ nm}^{-1}$, $\nu = 49.602 \text{ THz}$, (c) $\bar{q} = 0.01 \text{ nm}^{-1}$, $\nu = 49.217 \text{ THz}$, and (d) $\bar{q} = 0.05x \text{ nm}^{-1}$, $\nu = 50.002 \text{ THz}$. The maximum field values are set 1. (a)-(c) show that, at a fixed \bar{q} , the specific moiré pattern of EM waves is sensitive to the frequency. (a) and (d) (taken from the same branch) indicate that, as \bar{q} goes away from the light cone, the dominant PhP becomes more homogeneous or long-wavelength like [the ratio $r_b(\bar{q})$ becomes larger].

$Z_B = -Z_N \approx 2.7$ is assumed isotropic in this study [13]. We focus on the 2.65° twisted bilayer hBN. The moiré lattice length is $L_\theta \approx 5.42 \text{ nm}$ with 1876 atoms within each supercell. The long-wavelength dispersion near ω_0 is shown in Fig. 2. Due to the scattering and resonance, many PhP branches appear. According to our calculation, the phonon moiré potential, although weak in magnitude, could effectively hybridize the long-wavelength $\bar{q} \approx \mathbf{0}$ component with those of $\bar{q} + \mathbf{Q}$ ($\mathbf{Q} \neq \mathbf{0}$). The off-diagonal terms of the susceptibility Eq. (6) are non-negligible especially for ω near the resonance frequency $\omega_{\bar{q}b}$. It is such elements that provide PhPs with new branches and moiré patterns. The dispersions shuttle between different regions partitioned by the adjacent $\omega_{\bar{q}b}$. A dominant branch survives above 49.6 THz, which resembles the moiré-less TM mode. Because the moiré potential is weak, the folded phonon frequencies $\omega_{\bar{q}b}$ stay very close to each other. Therefore, the emerging moiré modes are quite flat (compared to the dominant mode), whose dispersions have tiny resolutions in the scale of 0.01 THz [Fig. 2(b)]. Therefore, the detection of moiré PhP dispersion becomes feasible only in samples exhibiting low dissipation, presenting experimental challenges. All the eigen modes are moiré PhPs, in the sense that

the eigen EM fields (and the lattice oscillation) have more or less components mixing between \bar{q} and $\bar{q} + \mathbf{Q}$ ($\mathbf{Q} \neq \mathbf{0}$), due to umklapp elastic scatterings. This results in the inhomogeneous optical response with the typical length scale $O(L_\theta)$. The EM fields of some modes are depicted in Fig. 3, where the formation of moiré patterns is clearly seen. We note that field components with wave vectors \bar{q} and $\bar{q} + \mathbf{Q}$ ($\mathbf{Q} \neq \mathbf{0}$) are distinguishable because they are localized around the material to different extent. Since $|\bar{q}|/|\mathbf{Q}| \ll 1$, the spatial range of \mathbf{Q} component along z -axis is $\lambda_{\mathbf{Q}}^{-1} \approx |\mathbf{Q}|^{-1} \sim L_\theta$, which is much shorter than that of the \bar{q} component. Besides, for each branch b , the ratio between the long- and short-wavelength components of the in-plane electric fields, quantified as $r_b(\bar{q}) = |\mathbf{E}_{\bar{q},t}|^2 / (\sum_{\mathbf{Q}} |\mathbf{E}_{\bar{q}+\mathbf{Q},t}|^2)$, changes continuously when \bar{q} goes away from the light cone. These characteristics could potentially act as experimental indicators in far-field settings in order to detect moiré PhPs.

Another emblematic character of moiré PhP is the inhomogeneous local response. This provides key clues for their detection using the scanning near-field optical microscope (SNOM) technique [37, 61]. In SNOM, a highly confined light $\mathbf{E} \sim \delta(\mathbf{r} - \mathbf{r}_0)e^{-i\omega t}$ is shed into the sam-

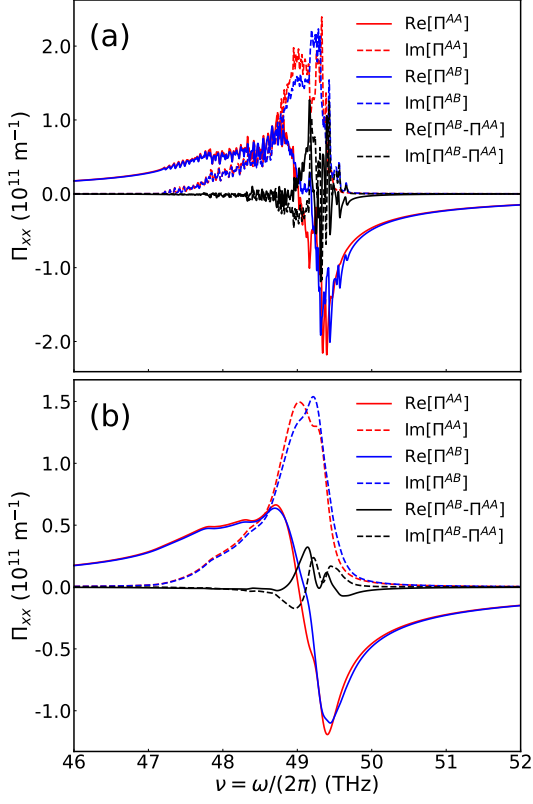


FIG. 4. The local susceptibility as a function of frequency, calculated using linewidth (a) $\delta/(2\pi) = 0.015$ THz (0.5 cm^{-1}) and (b) $\delta/(2\pi) = 0.15$ THz (5 cm^{-1}). The red and blue curves denote the values at AA and AB points, with solid and dashed lines representing the real and imaginary parts. The black lines indicate their difference.

ple, and the response at the same position \mathbf{r}_0 is collected. The local susceptibility $\mathbf{\Pi}(\mathbf{r}, \mathbf{r}, \omega)$ is responsible for such signals. In our formalism, this quantity can be calculated as (N_m is the number of supercells, see SI)

$$\mathbf{\Pi}(\mathbf{r}, \mathbf{r}, \omega) = \frac{1}{N_m \Omega_m} \sum_{\bar{\mathbf{q}} \mathbf{Q} \mathbf{Q}'} \mathbf{\Pi}^{\mathbf{Q} \mathbf{Q}'}(\bar{\mathbf{q}}, \omega) e^{i(\mathbf{Q} - \mathbf{Q}') \cdot \mathbf{r}}. \quad (9)$$

We see that a system has inhomogeneous local response, i.e., $\mathbf{\Pi}(\mathbf{r}, \mathbf{r}, \omega)$ depends explicitly on \mathbf{r} , if and only if $\mathbf{\Pi}^{\mathbf{Q} \mathbf{Q}'}(\bar{\mathbf{q}}, \omega)$ is not diagonal about \mathbf{Q} . This rules out the possibility to observe spatially varying signals in moiré-less systems such as a monolayer hBN. We numerically calculate Eq. (9) at two different stacking points, AA and AB, using a 7×7 sample mesh of $\bar{\mathbf{q}}$, 61 truncated \mathbf{Q} vectors, and two different phonon linewidth δ . The calculated Π_{xx} [Eq. (9) is found nearly isotropic: $\Pi_{xx} \approx \Pi_{yy}$, $\Pi_{xy} \approx \Pi_{yx} \approx 0$] in the frequency window $46 \sim 52$ THz is shown in Fig. 4. The sawtooth pattern appears in the susceptibility at both AA and AB points if the phonon linewidth $\delta/(2\pi) = 0.015$ THz is used, each indicating a specific moiré mode. The signal difference between AA and AB points occurs in a smaller window $48.5 \sim 50$ THz where the moiré polaritons are active [Fig. 2(a)].

The difference is tiny outside this range, as also indicated by Figs. 3(a) and (d). We also test a larger linewidth $\delta/(2\pi) = 0.15$ THz that is closer to experimental values. Although the sawtooth pattern disappears due to damping, we find the difference between responses at AA and AB points is still seizable. The numerical result is qualitatively consistent to previous SNOM experiments [37]. The resilient nature of moiré polar systems against damping manifests in the spatially varying near-field response, offering a robust experimental method for their detection.

The twisted bilayer MoTe₂ have arose wide interest since its experimental evidence of the fractional Chern insulating phase [26, 27]. The ions carry effective charges $Z_{\text{Mo}} = -2Z_{\text{Te}} \approx 3.16$ (obtained from DFT calculations), while the ionic mass are much larger than those of hBN, leading to a lower optical phonon frequency $\nu_0 \approx 7.2$ THz and weaker PhP dispersions. We calculate the PhP of 3.89° bilayer MoTe₂, and the result is shown in SI. Some basic properties are found qualitatively the same to the hBN. It will be interesting to study the interplay between moiré PhP and electrons in this fascinating system.

The phenomenological understanding of moiré PhP brings out a simple continuum model. In moiré-less case, only the $\mathbf{Q} = \mathbf{0}$ vibrational field \mathbf{W}_0 could couple to long-wavelength electric field, leading to a susceptibility Eq. (3) with a single pole. In the presence of moiré potential, the long-wavelength optical components are scattered and redistributed to other phonon branches, rendering the moiré susceptibility into Eq. (6) with many additional poles. A toy model of coupled harmonic oscillators helps understand the physics here (see SI and Ref. [32]). We take a step further to construct a continuum model for more quantitative analysis. In such model the vibrational field consists of different sub-fields in the l -th layer: $\mathbf{W} = \sum_{\mathbf{Q}l} \mathbf{W}_{\mathbf{Q}l} e^{i\mathbf{Q} \cdot \mathbf{r}}$, so do the electric and polarization fields. Each term $\mathbf{W}_{\mathbf{Q}l}$ ($\propto e^{i\bar{\mathbf{q}} \cdot \mathbf{r} - i\omega t}$) has a unique resonance frequency $\omega_{\mathbf{Q}l}$ and a commensurate wave vector \mathbf{Q} . These components are coupled to each other and to the electric field with the same wavelength

$$\ddot{\mathbf{W}}_{\mathbf{Q}l} = - \sum_{\mathbf{Q}'l'} \mathcal{D}_{\mathbf{Q}l, \mathbf{Q}'l'} \mathbf{W}_{\mathbf{Q}'l'} + \gamma \mathbf{E}_{\mathbf{Q}}, \quad (10)$$

and the polarization field

$$\mathbf{P} = \sum_{\mathbf{Q}} \mathbf{P}_{\mathbf{Q}} e^{i\mathbf{Q} \cdot \mathbf{r}} = \sum_{\mathbf{Q}l} \gamma \mathbf{W}_{\mathbf{Q}l} e^{i\mathbf{Q} \cdot \mathbf{r}}. \quad (11)$$

The charge parameter γ is the same as γ_{12} in Eq. (1). The coupling matrix \mathcal{D} is obtained through the projection of the lattice dynamical matrix, and is retained to be nonzero only for nearest components: $|\mathbf{Q} - \mathbf{Q}'| \leq 4\pi/(\sqrt{3}L_\theta)$ (see SI). The diagonal terms $\mathcal{D}_{\mathbf{Q}l, \mathbf{Q}l}$ contain just the monolayer phonon frequencies $\omega_{\mathbf{Q}l}$. The off-diagonal terms $\mathcal{D}_{\mathbf{Q}l, \mathbf{Q}'l'}$ scatter vibrational sub-fields with different wave vectors. This model generalizes the Huang's equations Eqs. (1), (2) for the moiré case. It is much more computationally efficient than the lattice

model since it contains only several model parameters and makes a cutoff on Q [62]. In general \mathcal{D} depends largely on lattice relaxations, which is dominant in moiré systems with larger supercells. We will use this model to systematically study them in the future.

Summary and outlooks. Following the spirit of Huang’s theory, a set of macroscopic equations is summarized that helps understand how 2D PhP exists. For moiré systems, the eigen equation couples different momentum together, resulting in multiple branches of inhomogeneous PhP modes with moiré patterns. The theoretical proposal is numerically verified using the lattice model. Many PhP bands are observed, each carrying a unique EM wave that is polarized and localized differently. The inhomogeneous multi-branch physics could be understood by generalizing Huang’s theory to those of coupled harmonic oscillators. In this tentative study, we only calculate two specific moiré systems with relatively small supercells. There is still plenty of room to explore the optical dependence on material parameters. For ex-

ample, samples with supercells comparable to reachable light wavelength are more charming for experiments [37]. The spatial localization of EM waves, and the tunability of their wavelength and frequency, are fascinating features of 2D optics. If such modes can be excited relentlessly, they could provide flexible driven potentials that are completely different with traditional light fields [59, 63]. We leave these explorations in future studies.

ACKNOWLEDGMENTS

We thank X.-D. Guo, W.-Q. Miao, and T.-Y. Qiao for helpful discussions. X. Dai is supported by a fellowship and a CRF award from the Research Grants Council of the Hong Kong Special Administrative Region, China (Projects No. HKUST SRFS2324-6S01 and No. C7037-22GF). D. Pan is supported by National Natural Science Foundation of China through the Excellent Young Scientists Fund (22022310).

-
- [1] Q. Zhang, G. Hu, W. Ma, P. Li, A. Krasnok, R. Hillenbrand, A. Alù, and C.-W. Qiu, *Nature* **597**, 187 (2021).
- [2] D. L. Chafatinos, A. S. Kuznetsov, S. Anguiano, A. E. Bruchhausen, A. A. Reynoso, K. Biermann, P. V. Santos, and A. Fainstein, *Nature Communications* **11**, 4552 (2020).
- [3] T. P. Lyons, D. J. Gillard, C. Leblanc, J. Puebla, D. D. Solnyshkov, L. Klompmaker, I. A. Akimov, C. Louca, P. Muduli, A. Genco, M. Bayer, Y. Otani, G. Malpuech, and A. I. Tartakovskii, *Nature Photonics* **16**, 632 (2022).
- [4] D. N. Basov, M. M. Fogler, and F. J. G. de Abajo, *Science* **354**, aag1992 (2016), <https://www.science.org/doi/pdf/10.1126/science.aag1992>.
- [5] S. Ghosh and T. C. H. Liew, *npj Quantum Information* **6**, 16 (2020).
- [6] A. Kavokin, T. C. H. Liew, C. Schneider, P. G. Lagoudakis, S. Klemmt, and S. Hoefling, *Nature Reviews Physics* **4**, 435 (2022).
- [7] M. Born and K. Huang, *Dynamical Theory Of Crystal Lattices* (Oxford University Press, 1996).
- [8] T. Low, A. Chaves, J. D. Caldwell, A. Kumar, N. X. Fang, P. Avouris, T. F. Heinz, F. Guinea, L. Martin-Moreno, and F. Koppens, *Nature Materials* **16**, 182 (2017).
- [9] L. Du, M. R. Molas, Z. Huang, G. Zhang, F. Wang, and Z. Sun, *Science* **379**, eadg0014 (2023).
- [10] T. Sohler, M. Gibertini, M. Calandra, F. Mauri, and N. Marzari, *Nano Letters* **17**, 3758 (2017).
- [11] N. Rivera, T. Christensen, and P. Narang, *Nano Letters* **19**, 2653 (2019).
- [12] Z. Yuan, R. Chen, P. Li, A. Y. Nikitin, R. Hillenbrand, and X. Zhang, *ACS Photonics* **7**, 2610 (2020).
- [13] D. M. Juraschek and P. Narang, *Nano Letters* **21**, 5098 (2021).
- [14] N. Li, X. Guo, X. Yang, R. Qi, T. Qiao, Y. Li, R. Shi, Y. Li, K. Liu, Z. Xu, L. Liu, F. J. García de Abajo, Q. Dai, E.-G. Wang, and P. Gao, *Nature Materials* **20**, 43 (2021).
- [15] J. Li, L. Wang, Y. Wang, Z. Tao, W. Zhong, Z. Su, S. Xue, G. Miao, W. Wang, H. Peng, J. Guo, and X. Zhu, *Nature Communications* **15**, 1938 (2024).
- [16] L. Wendler and E. Jäger, *physica status solidi (b)* **120**, 235 (1983).
- [17] C. Ding, Y. Du, and M. Zhao, *Phys. Rev. B* **109**, 125431 (2024).
- [18] L. Cavicchi, I. Torre, P. Jarillo-Herrero, F. H. L. Koppens, and M. Polini, *Phys. Rev. B* **110**, 045431 (2024).
- [19] G. Hu, Q. Ou, G. Si, Y. Wu, J. Wu, Z. Dai, A. Krasnok, Y. Mazor, Q. Zhang, Q. Bao, C.-W. Qiu, and A. Alù, *Nature* **582**, 209 (2020).
- [20] Y. Cao, V. Fatemi, S. Fang, K. Watanabe, T. Taniguchi, E. Kaxiras, and P. Jarillo-Herrero, *Nature* **556**, 43 (2018).
- [21] Y. Cao, V. Fatemi, A. Demir, S. Fang, S. L. Tomarken, J. Y. Luo, J. D. Sanchez-Yamagishi, K. Watanabe, T. Taniguchi, E. Kaxiras, R. C. Ashoori, and P. Jarillo-Herrero, *Nature* **556**, 80 (2018).
- [22] J. M. Park, Y. Cao, K. Watanabe, T. Taniguchi, and P. Jarillo-Herrero, *Nature* **590**, 249 (2021).
- [23] Y. Xu, S. Liu, D. A. Rhodes, K. Watanabe, T. Taniguchi, J. Hone, V. Elser, K. F. Mak, and J. Shan, *Nature* **587**, 214 (2020).
- [24] T. Han, Z. Lu, G. Scuri, J. Sung, J. Wang, T. Han, K. Watanabe, T. Taniguchi, H. Park, and L. Ju, *Nature Nanotechnology* **19**, 181 (2024).
- [25] M. Serlin, C. L. Tschirhart, H. Polshyn, Y. Zhang, J. Zhu, K. Watanabe, T. Taniguchi, L. Balents, and A. F. Young, *Science* **367**, 900 (2020).
- [26] J. Cai, E. Anderson, C. Wang, X. Zhang, X. Liu, W. Holtzmann, Y. Zhang, F. Fan, T. Taniguchi, K. Watanabe, Y. Ran, T. Cao, L. Fu, D. Xiao, W. Yao, and X. Xu, *Nature* **622**, 63 (2023).
- [27] K. Kang, B. Shen, Y. Qiu, Y. Zeng, Z. Xia, K. Watanabe, T. Taniguchi, J. Shan, and K. F. Mak, *Nature* **628**, 522 (2024).
- [28] T. Stauber, P. San-Jose, and L. Brey, *New Journal of*

- Physics **15**, 113050 (2013).
- [29] T. Stauber and H. Kohler, *Nano Letters* **16**, 6844 (2016).
- [30] X. Kuang, Z. Zhan, and S. Yuan, *Phys. Rev. B* **103**, 115431 (2021).
- [31] M. Papaj and C. Lewandowski, *Science Advances* **9**, eadg3262 (2023).
- [32] L. Zhang, F. Wu, S. Hou, Z. Zhang, Y.-H. Chou, K. Watanabe, T. Taniguchi, S. R. Forrest, and H. Deng, *Nature* **591**, 61 (2021).
- [33] J. M. Fitzgerald, J. J. P. Thompson, and E. Malic, *Nano Letters* **22**, 4468 (2022).
- [34] K. W. Song and O. Kyriienko, “Electrically tunable and enhanced nonlinearity of moiré exciton-polaritons in transition metal dichalcogenide bilayers,” (2024), [arXiv:2406.08263](https://arxiv.org/abs/2406.08263) [cond-mat.mes-hall].
- [35] W. Miao, C. Li, X. Han, D. Pan, and X. Dai, *Phys. Rev. B* **107**, 125112 (2023).
- [36] H. Shi, W. Miao, and X. Dai, “Moiré optical phonons dancing with heavy electrons in magic-angle twisted bilayer graphene,” (2024), [arXiv:2402.11824](https://arxiv.org/abs/2402.11824) [cond-mat.mes-hall].
- [37] S. L. Moore, C. J. Ciccarino, D. Halbertal, L. J. McGilly, N. R. Finney, K. Yao, Y. Shao, G. Ni, A. Sternbach, E. J. Telford, B. S. Kim, S. E. Rossi, K. Watanabe, T. Taniguchi, A. N. Pasupathy, C. R. Dean, J. Hone, P. J. Schuck, P. Narang, and D. N. Basov, *Nature Communications* **12**, 5741 (2021).
- [38] V. Falko and D. Khmel'nitskii, *Zh. Eksp. Teor. Fiz* **95**, 847 (1989).
- [39] K. L. Kliewer and R. Fuchs, *Phys. Rev.* **144**, 495 (1966).
- [40] K. L. Kliewer and R. Fuchs, *Phys. Rev.* **150**, 573 (1966).
- [41] S. A. Mikhailov and K. Ziegler, *Phys. Rev. Lett.* **99**, 016803 (2007).
- [42] S. G. Menabde, D. R. Mason, E. E. Kornev, C. Lee, and N. Park, *Scientific Reports* **6**, 21523 (2016).
- [43] F. Stern, *Phys. Rev. Lett.* **18**, 546 (1967).
- [44] P. A. D. Gonçalves and N. M. Peres, *An introduction to graphene plasmonics* (World Scientific, 2016).
- [45] X. Gonze and C. Lee, *Phys. Rev. B* **55**, 10355 (1997).
- [46] J. Tersoff, *Phys. Rev. B* **37**, 6991 (1988).
- [47] A. N. Kolmogorov and V. H. Crespi, *Phys. Rev. B* **71**, 235415 (2005).
- [48] W. Ouyang, D. Mandelli, M. Urbakh, and O. Hod, *Nano Letters* **18**, 6009 (2018).
- [49] W. Ouyang, I. Azuri, D. Mandelli, A. Tkatchenko, L. Kronik, M. Urbakh, and O. Hod, *Journal of Chemical Theory and Computation* **16**, 666 (2020).
- [50] F. H. Stillinger and T. A. Weber, *Phys. Rev. B* **31**, 5262 (1985).
- [51] J.-W. Jiang, *Nanotechnology* **26**, 315706 (2015).
- [52] W. Ouyang, R. Sofer, X. Gao, J. Hermann, A. Tkatchenko, L. Kronik, M. Urbakh, and O. Hod, *Journal of Chemical Theory and Computation* **17**, 7237 (2021).
- [53] W. Jiang, R. Sofer, X. Gao, A. Tkatchenko, L. Kronik, W. Ouyang, M. Urbakh, and O. Hod, *The Journal of Physical Chemistry A* **127**, 9820 (2023).
- [54] A. P. Thompson, H. M. Aktulga, R. Berger, D. S. Bolinteanu, W. M. Brown, P. S. Crozier, P. J. in 't Veld, A. Kohlmeyer, S. G. Moore, T. D. Nguyen, R. Shan, M. J. Stevens, J. Tranchida, C. Trott, and S. J. Plimpton, *Computer Physics Communications* **271**, 108171 (2022).
- [55] N. Rivera, J. Coulter, T. Christensen, and P. Narang, “Ab initio calculation of phonon polaritons in silicon carbide and boron nitride,” (2018), [arXiv:1809.00058](https://arxiv.org/abs/1809.00058) [physics.optics].
- [56] T. Sohler, M. Calandra, and F. Mauri, *Phys. Rev. B* **94**, 085415 (2016).
- [57] N. Wiser, *Phys. Rev.* **129**, 62 (1963).
- [58] X. Wang, C. Xu, S. Aronson, D. Bennett, N. Paul, P. J. D. Crowley, C. Collignon, K. Watanabe, T. Taniguchi, R. Ashoori, E. Kaxiras, Y. Zhang, P. Jarillo-Herrero, and K. Yasuda, “Band structure engineering using a moiré polar substrate,” (2024), [arXiv:2405.03761](https://arxiv.org/abs/2405.03761) [cond-mat.mes-hall].
- [59] K. Han, M. Cho, T. Kim, S. T. Kim, S. H. Kim, S. H. Park, S. M. Yang, K. Watanabe, T. Taniguchi, V. Menon, and Y. D. Kim, “Highly tunable moiré superlattice potentials in twisted hexagonal boron nitrides,” (2024), [arXiv:2410.22593](https://arxiv.org/abs/2410.22593) [cond-mat.mes-hall].
- [60] S. Dai, Z. Fei, Q. Ma, A. S. Rodin, M. Wagner, A. S. McLeod, M. K. Liu, W. Gannett, W. Regan, K. Watanabe, T. Taniguchi, M. Thiemens, G. Dominguez, A. H. C. Neto, A. Zettl, F. Keilmann, P. Jarillo-Herrero, M. M. Fogler, and D. N. Basov, *Science* **343**, 1125 (2014).
- [61] X. Guo, N. Li, X. Yang, R. Qi, C. Wu, R. Shi, Y. Li, Y. Huang, F. J. García de Abajo, E.-G. Wang, P. Gao, and Q. Dai, *Nature Nanotechnology* **18**, 529 (2023).
- [62] R. Bistritzer and A. H. MacDonald, *Proceedings of the National Academy of Sciences* **108**, 12233 (2011), <https://www.pnas.org/doi/pdf/10.1073/pnas.1108174108>.
- [63] Q. Gao and Q. Niu, *Phys. Rev. Lett.* **127**, 036401 (2021).

SUPPLEMENTARY INFORMATION

CONTENTS

Acknowledgments	6
References	6
Supplementary information	8
A. Macroscopic theory of 2D PhP	8
1. Huang's equation in 2D	8
2. Non-retarded solutions	9
3. Guided modes: 2D EM	10
4. Radiative solutions: 3D EM	11
5. Revisit 2D PhP as a light reflection and refraction problem	11
B. Lattice model of 2D PhP in simple polar systems	12
1. Lattice dynamics of 2D polar systems	12
2. Relation to the macroscopic theory	13
3. Force constant of monolayer hBN	15
C. Lattice model of 2D PhP in moiré polar systems	16
1. Equation of motion and polarization in moiré superlattice	16
2. Moiré polaritons	18
D. Macroscopic theory of moiré PhP	20
1. A toy model: coupled harmonic oscillators	20
2. The continuum model for moiré phonon	20
3. The continuum model for moiré PhP	23
E. More details about the moiré response function	24
1. Derivation in quantum case	24
2. Non-locality and inhomogeneity	25
3. Symmetry properties	26
4. Representation in moiré-less basis	26
F. Interatomic force constant	27

Appendix A: Macroscopic theory of 2D PhP

1. Huang's equation in 2D

Consider a 2D polar sheet placed at $z = 0$ of a dielectric with permittivity $\epsilon_0\epsilon$ (in this SI we generalize the vacuum case) and permeability $\mu = 1$ [Fig. 1(a) of the main text]. We import a continuum vibrational field \mathbf{W} defined in the plane. For diatomic ionic crystals like hBN it is connected to the ion displacements through $\mathbf{W} \propto \mathbf{u}_+ - \mathbf{u}_-$. With electric field \mathbf{E} , \mathbf{W} satisfies the equation of motion of a driven oscillator (neglect dissipation)

$$\ddot{\mathbf{W}} = -\omega_0^2 \mathbf{W} + \gamma_{12} \mathbf{E}_t, \quad (\text{A1})$$

where ω_0 is the optical phonon frequency resulting from elastic forces, \mathbf{E}_t is the in-plane part of \mathbf{E} at $z = 0$. The surface polarization density (in-plane dipole moment per unit area) is denoted by \mathbf{P} . In 2D it originates mainly from the ionic displacement (rigid-ion approximation)

$$\mathbf{P} = \gamma_{21} \mathbf{W}. \quad (\text{A2})$$

The parameters $\gamma_{12} = \gamma_{21}$ due to Onsager relations (or can be inferred from microscopic models). For clarity we set $\gamma_{12}^2 = \gamma_{21}^2 = \epsilon_0 T$. The above two equations are 2D version of Huang's equations. Their microscopic origin is derived

in Sec. B2. They should be solved together with Maxwell's equations, which govern the form of EM waves in the dielectric $z \neq 0$ and reduce to boundary conditions (BC) at $z = 0$:

$$\text{1st : } \mathbf{E}_t^+ - \mathbf{E}_t^- = \mathbf{0}, \quad (\text{A3a})$$

$$\text{2nd : } \epsilon_0 \epsilon (E_z^+ - E_z^-) = \rho, \quad (\text{A3b})$$

$$\text{3rd : } \mathbf{B}_t^+ - \mathbf{B}_t^- = \mu_0 \mathbf{J} \times \mathbf{e}_z, \quad (\text{A3c})$$

$$\text{4th : } B_z^+ - B_z^- = 0, \quad (\text{A3d})$$

where ρ and \mathbf{J} are surface charge and current densities, and ‘ \pm ’ indicates fields just above or below the sheets, e.g., $\mathbf{E}^\pm = \mathbf{E}(z = 0^\pm)$. We study solutions of the form

$$\mathbf{E}, \mathbf{W} \propto e^{i\mathbf{q}\cdot\mathbf{r} - i\omega t}, \quad (\text{A4})$$

where $\mathbf{r} = (x, y)$ and \mathbf{q} are *in-plane* position and momentum, respectively. The in-plane dipole current and charge density

$$\mathbf{J} = \partial \mathbf{P} / \partial t = -i\omega \mathbf{P}, \quad \rho = -i\mathbf{q} \cdot \mathbf{P}. \quad (\text{A5})$$

Then the 2nd and 3rd BCs become

$$\epsilon_0 \epsilon (E_z^+ - E_z^-) = -i\mathbf{q} \cdot \mathbf{P}, \quad (\text{A6})$$

$$\partial_z \mathbf{E}_t^+ - \partial_z \mathbf{E}_t^- - i\mathbf{q} (E_z^+ - E_z^-) = -\mu_0 \omega^2 \mathbf{P}, \quad (\text{A7})$$

while the 4th BC coincides with the 1st one. In dielectric ($z \neq 0$) the \mathbf{E} field obeys the divergence law and the wave equation

$$\nabla \cdot \mathbf{E} = i\mathbf{q} \cdot \mathbf{E}_t + \partial_z E_z = 0, \quad (\text{A8})$$

$$(\nabla^2 - \epsilon \partial_t^2) \mathbf{E} = \left(\partial_z^2 - q^2 + \epsilon \frac{\omega^2}{c^2} \right) \mathbf{E} = \mathbf{0}. \quad (\text{A9})$$

Depending on the sign of

$$\lambda^2 = q^2 - \epsilon \frac{\omega^2}{c^2}, \quad (\text{A10})$$

the solutions can be divided into guided or radiative modes. At $\omega \neq \omega_0$, the susceptibility can be defined

$$\mathbf{P} = \epsilon_0 \Pi(\omega) \mathbf{E}_t, \quad \Pi(\omega) = \frac{T}{\omega_0^2 - \omega^2}. \quad (\text{A11})$$

2. Non-retarded solutions

Let us first take a look at the non-retarded (static) limit without *external* field. In this limit, c is set infinity, so $\lambda = q$. Also we only need to consider the 1st and 2nd BCs. At $q = 0$, pure oscillation $\mathbf{W} \neq \mathbf{0}$ happens and $\mathbf{E} = \mathbf{0}$, with the transverse and longitudinal oscillations sharing the same frequency ω_0 . For $q > 0$, the transverse pure oscillation with frequency ω_0 is still a solution, but the longitudinal mode will move with built-in electric field. For longitudinal mode, \mathbf{E}_t has nonzero longitudinal component E_{\parallel} . Suppose $E_{\parallel} \propto e^{i\mathbf{q}\cdot\mathbf{r} - \lambda|z| - i\omega t}$. In static limit, Eq. (A8) gives $E_z^\pm = \pm iE_{\parallel}$, and the 2nd BC gives $2iE_{\parallel} = -iqP_{\parallel}/(\epsilon_0\epsilon)$. Combined with Eq. (A11), we get the static longitudinal mode condition:

$$1 + \frac{q}{2\epsilon} \Pi(\omega) = 0, \quad (\text{A12})$$

from which we get the longitudinal dispersion

$$\omega = \omega_0 \sqrt{1 + \frac{qT}{2\epsilon\omega_0^2}} \approx \omega_0 + \frac{qT}{4\epsilon\omega_0}. \quad (\text{A13})$$

The static transverse and longitudinal phonon dispersions are shown in Fig. 1(b) of the main text using dashed lines. We see the above model, although simple, captures both the degeneracy of TO and LO phonons at Γ point and the linear LO-TO splitting in the long-wavelength regime, which are typical properties of 2D polar systems [10, 11, 15]. We notice that only in the non-retarded limit, the condition (A12) for LO phonon coincides with that for the 2D TM polariton studied before [11, 13].

3. Guided modes: 2D EM

First let's focus on the regime $\lambda^2 > 0$. We focus on the case $\omega \neq \omega_0$, where Eq. (A11) can be used to eliminate \mathbf{W} ($\omega = \omega_0$ leads to the trivial solution $\mathbf{W} = \mathbf{E} = \mathbf{0}$). Set $\lambda = \sqrt{q^2 - \varepsilon\omega^2/c^2} > 0$, we may assume the following localized \mathbf{E} field

$$\mathbf{E}(\mathbf{r}, z, t) = \begin{cases} (\mathbf{E}_t + E_z^+ \mathbf{e}_z) e^{i\mathbf{q}\cdot\mathbf{r} - \lambda z - i\omega t} & z > 0 \\ (\mathbf{E}_t + E_z^- \mathbf{e}_z) e^{i\mathbf{q}\cdot\mathbf{r} + \lambda z - i\omega t} & z < 0 \end{cases}, \quad (\text{A14})$$

where $\mathbf{E}_t = E_{\parallel} \mathbf{e}_q + E_{\perp} \mathbf{e}_z \times \mathbf{e}_q$, \mathbf{e}_q is the unit vector along \mathbf{q} . The divergence theorem gives

$$E_z^+ = -E_z^- = iqE_{\parallel}/\lambda. \quad (\text{A15})$$

The 2nd BC (A6) becomes

$$2\frac{iqE_{\parallel}}{\lambda} = -\frac{iqP_{\parallel}}{\epsilon_0\epsilon} \Rightarrow \left[1 + \frac{\lambda}{2\varepsilon}\Pi(\omega)\right] E_{\parallel} = 0, \quad (\text{A16})$$

The longitudinal part of the 3rd BC (A7) is equivalent to the 2nd one, while the transverse part reads

$$2\lambda q E_{\perp} = \mu_0 \omega^2 q P_{\perp} \Rightarrow \left[1 - \frac{1}{2\lambda} \frac{\omega^2}{c^2} \Pi(\omega)\right] E_{\perp} = 0. \quad (\text{A17})$$

We see the solutions are decoupled in E_{\parallel} and E_{\perp} in this isotropic toy model. In realistic models especially moiré materials, they will in general be coupled.

Consider first the case $E_{\parallel} \neq 0$, $E_{\perp} = 0$. This gives a \mathbf{B} field polarized perpendicular to \mathbf{e}_q ,

$$\begin{aligned} \mathbf{E}^{\pm} &= \left(E_{\parallel} \mathbf{e}_q \pm i\frac{q}{\lambda} E_{\parallel} \mathbf{e}_z\right) e^{i\mathbf{q}\cdot\mathbf{r} - i\omega t - \lambda|z|}, \\ \mathbf{B}^{\pm} &= \mp i\frac{\omega\varepsilon}{\lambda c^2} E_{\parallel} \mathbf{e}_z \times \mathbf{e}_q e^{i\mathbf{q}\cdot\mathbf{r} - i\omega t - \lambda|z|}, \end{aligned} \quad (\text{A18})$$

which is the transverse magnetic (TM) mode. In this case the eigen equation reduces to the TM mode condition

$$\text{TM: } 1 + \frac{\lambda}{2\varepsilon}\Pi(\omega) = 0. \quad (\text{A19})$$

Since $\lambda > 0$, it has solution when $\Pi(\omega) < 0$, i.e., when $\omega > \omega_0$. The dispersion reads

$$q = \sqrt{\varepsilon \frac{\omega^2}{c^2} + \varepsilon^2 \frac{(\omega^2 - \omega_0^2)^2}{T^2/4}}. \quad (\text{A20})$$

At $\omega = \omega_0$, $q = q_0 = \sqrt{\varepsilon}\omega_0/c$, the group velocity $v_0 = d\omega/dq|_{q=q_0} = c/\sqrt{\varepsilon}$, i.e., the TM mode is tangential to the light cone. As shown in Fig. 1(b), when $q \gg q_0$, the dispersion becomes linear and asymptotic with respect to the static LO mode Eq. (A13).

Then consider the case $E_{\parallel} = 0$, $E_{\perp} \neq 0$, which corresponds to the transverse electric (TE) mode

$$\begin{aligned} \mathbf{E}^{\pm} &= E_{\perp} \mathbf{e}_z \times \mathbf{e}_q e^{i\mathbf{q}\cdot\mathbf{r} - i\omega t - \lambda|z|}, \\ \mathbf{B}^{\pm} &= \left(\pm \frac{\lambda}{i\omega} E_{\perp} \mathbf{e}_q + \frac{q}{\omega} E_{\perp} \mathbf{e}_z\right) e^{i\mathbf{q}\cdot\mathbf{r} - i\omega t - \lambda|z|}. \end{aligned} \quad (\text{A21})$$

The dispersion obeys the TE mode condition

$$\text{TE: } 1 - \frac{1}{2\lambda} \frac{\omega^2}{c^2} \Pi(\omega) = 0, \quad (\text{A22})$$

which has solutions when $\Pi(\omega) > 0$, i.e., when $\omega < \omega_0$. The dispersion reads

$$q = \frac{\omega}{c} \sqrt{\varepsilon + \frac{\omega^2}{c^2} \frac{T^2/4}{(\omega_0^2 - \omega^2)^2}}. \quad (\text{A23})$$

When $q < q_0$, the TE mode resembles light: the dispersion grows closely to the light cone, hence with a tiny λ and weak localization. When $q > q_0$, it turns almost into pure lattice oscillations: the dispersion stays intimately below the static TO line $\omega = \omega_0$ and the EM fields are weak and extremely localized at the surface.

The above TM and TE modes are typical 2D EM waves with their energy constrained in z -axis. Such modes, accompanied by polarizable collective modes, exist ubiquitously at 2D materials or interfaces of 3D materials. The eigenmode conditions (A19), (A22) are general to use, e.g., when discussing 2D plasmon polaritons one only needs to replace $\Pi(\omega)$ by its plasmon version. The rule is true as well that the sign of $\Pi(\omega)$ governs the TM or TE nature.

4. Radiative solutions: 3D EM

Then we consider the case $\lambda^2 < 0$, i.e., the left side of the light cone. This means the wave vector along z -axis is real, and we take $\lambda = -i\sqrt{\varepsilon\omega^2/c^2 - q^2} = -ik_z$. In other words, EM fields occupy the whole 3D space without decaying. In this case, we can no longer expect the existence of mono-directional waves in both $z > 0$ and $z < 0$ regions like Eq. (A14). Otherwise, if $\mathbf{E}^\pm = (\mathbf{E}_t + E_z^\pm \mathbf{e}_z)e^{i\mathbf{q}\cdot\mathbf{r} \pm ik_z z - i\omega t}$, following the derivation for $\lambda^2 > 0$ case, the resulting eigen equations are the same to Eqs. (A19) and (A22), which has no solution since λ is imaginary. Or, if we take $\mathbf{E}^\pm = (\mathbf{E}_t + E_z^\pm \mathbf{e}_z)e^{i\mathbf{q}\cdot\mathbf{r} + ik_z z - i\omega t}$, then $E_z^+ = E_z^-$. The 3rd BC gives $\mathbf{P} = \mathbf{0}$ and thus $\mathbf{W}_t = \mathbf{E} = \mathbf{0}$, which is also trivial. Instead, the \mathbf{E} field should be multi-directional at least in one half space. A typical solution is the light incidence setup treating the 2D sheet as a scattering potential, where in the half space of light source, plane waves are propagating along two directions. For this setup, in general for all (\mathbf{q}, ω) , non-trivial solution exists, corresponding to the continuous spectrum in the dispersion plots. We will solve them in next subsection, where the light incidence setup is generalized to contain both guided and radiative modes.

5. Revisit 2D PhP as a light reflection and refraction problem

Both the localized and radiative modes can be understood from the light reflection and refraction viewpoint. More importantly, it is directly connected to the experimental means to excite them, and is of better numerical convenience to reveal the dispersions. We denote the incident, reflected, and refracted light as \mathbf{E}^i , \mathbf{E}^r , and \mathbf{E}^t . Then we assume the light is incident from $z < 0$,

$$\begin{aligned} \mathbf{E}^i &= (\mathbf{E}_t^i + iqE_{\parallel}^i/\lambda\mathbf{e}_z)e^{i\mathbf{q}\cdot\mathbf{r} - \lambda z - i\omega t}, \\ \mathbf{E}^r &= (\mathbf{E}_t^r - iqE_{\parallel}^r/\lambda\mathbf{e}_z)e^{i\mathbf{q}\cdot\mathbf{r} + \lambda z - i\omega t}, \\ \mathbf{E}^t &= (\mathbf{E}_t^t + iqE_{\parallel}^t/\lambda\mathbf{e}_z)e^{i\mathbf{q}\cdot\mathbf{r} - \lambda z - i\omega t}, \end{aligned} \quad (\text{A24})$$

where the in-plane part $\mathbf{E}_t^l = E_{\parallel}^l \mathbf{e}_q + E_{\perp}^l \mathbf{e}_z \times \mathbf{e}_q$, $l = i, r, t$. Here λ are allowed to take real or imaginary values,

$$\lambda = \begin{cases} -i\sqrt{\varepsilon\frac{\omega^2}{c^2} - q^2}, & q < \sqrt{\varepsilon}\omega/c \\ \sqrt{q^2 - \varepsilon\frac{\omega^2}{c^2}}, & q > \sqrt{\varepsilon}\omega/c \end{cases}, \quad (\text{A25})$$

depending on whether the EM wave is radiative or guided. Notice that in the guided case the incidence should also be attenuated, which can be generated using the Otto configuration [44]. Then the 1st BC reads

$$\mathbf{E}_t^t = \mathbf{E}_t^i + \mathbf{E}_t^r. \quad (\text{A26})$$

The 2nd BC reads

$$\mathbf{e}_q \cdot \left[\mathbf{E}_t^t - \mathbf{E}_t^i + \mathbf{E}_t^r + \frac{\lambda}{\varepsilon}\Pi(\omega)\mathbf{E}_t^t \right] = 0. \quad (\text{A27})$$

The longitudinal part of the 3rd BC is still equivalent to the above one, and the transverse part reads

$$\mathbf{e}_q \times \left[\mathbf{E}_t^t - \mathbf{E}_t^i + \mathbf{E}_t^r - \frac{1}{\lambda}\frac{\omega^2}{c^2}\Pi(\omega)\mathbf{E}_t^t \right] = 0. \quad (\text{A28})$$

From the above equations, we can express \mathbf{E}^t and \mathbf{E}^r using the incident light \mathbf{E}^i ,

$$\mathbf{E}_t^t = T(\mathbf{q}, \omega)\mathbf{E}_t^i, \quad \mathbf{E}_t^r = R(\mathbf{q}, \omega)\mathbf{E}_t^i, \quad (\text{A29})$$

and the transmission and reflection matrices are (written in the basis of E_{\parallel}^l , E_{\perp}^l , I is the identity)

$$T(\mathbf{q}, \omega) = \begin{pmatrix} 1 + \frac{\lambda}{2\varepsilon}\Pi(\omega) & \\ & 1 - \frac{1}{2\lambda}\frac{\omega^2}{c^2}\Pi(\omega) \end{pmatrix}^{-1}, \quad (\text{A30a})$$

$$R(\mathbf{q}, \omega) = T(\mathbf{q}, \omega) - I. \quad (\text{A30b})$$

When (\mathbf{q}, ω) lives in the radiative regime, the above equation describes a usual transmission and reflection problem discussed in Sec. A4. When (\mathbf{q}, ω) lives in the guided regime, T , R have poles corresponding exactly to the polariton dispersion discussed in Sec. A3. Poles indicate that E^t and E^r can be induced with infinitesimal incidence E^i , hinting the excitation of intrinsic mode. We can make both the continuous spectrum and the discrete dispersion visual by plotting the transmission spectrum

$$\mathcal{L}(\mathbf{q}, \omega) = -\text{Im}[\det[T(\mathbf{q}, \omega + i\delta)]], \quad (\text{A31})$$

where the phonon linewidth δ is tiny and positive.

In this section we discuss only about the moiré-less case. In moiré materials or hetero structures, multi-pole response should be incorporated into Eqs. (A1), (A2) to correctly describe the long-wavelength behavior. We leave such generalization in Sec. D.

Appendix B: Lattice model of 2D PhP in simple polar systems

1. Lattice dynamics of 2D polar systems

In this section we build the lattice theory for 2D polar systems. We still focus on the moiré-less case in this section, but it will be generalized to contain moiré effects in the next section. In such model the short-ranged force among ions are described by the force constant $\Phi_{\alpha,\beta}$ introduced in Sec. F, while the long-ranged Coulomb force (specifically, dipole-dipole interaction) are incorporated into macroscopic electric fields. In the long-wavelength limit, it should reduce to the macroscopic Huang's theory introduced in Sec. A1.

Suppose we have a lattice where the ions' equilibrium positions are $\mathbf{r}_{i\alpha} = \mathbf{R}_i + \boldsymbol{\tau}_{\alpha}$, where \mathbf{R}_i denotes the i -th unit cell, $\boldsymbol{\tau}_{\alpha}$ denotes the relative position of sublattice α . With the long-wavelength electric field $\mathbf{E}(\mathbf{r}) = \mathbf{E}_{\mathbf{q}}(\omega)e^{i\mathbf{q}\cdot\mathbf{r}-i\omega t}$ ($\mathbf{q} \approx \mathbf{0}$), the equation of motion for lattice displacement $\mathbf{u}(\mathbf{r}_{i\alpha})$ is (we focus on in-plane dynamics in this study, so μ, ν takes x, y only)

$$M_{\alpha}\ddot{u}_{\mu}(\mathbf{r}_{i\alpha}) + \sum_{j\beta\nu} \Phi_{\alpha\mu,\beta\nu}(\mathbf{r}_{i\alpha} - \mathbf{r}_{j\beta})u_{\nu}(\mathbf{r}_{j\beta}) - Z_{\alpha}eE_{\mathbf{q},\mu}(\omega)e^{i\mathbf{q}\cdot\mathbf{r}_{i\alpha}-i\omega t} = 0, \quad (\text{B1})$$

where Z_{α} and M_{α} are effective (dimensionless) charge and mass (which are assumed isotropic) of sublattice α , e is the elementary charge, and $\Phi_{\alpha,\beta}$ is the lattice constant for nearby ions. In the absence of \mathbf{E} , the above equation reduces just to the harmonic equation of motion in the usual phonon problem. The polarization density is defined as [7, 55]

$$\mathbf{P}(\mathbf{r}) = \sum_{i\alpha} Z_{\alpha}e\mathbf{u}(\mathbf{r}_{i\alpha})\delta(\mathbf{r} - \mathbf{r}_{i\alpha}), \quad (\text{B2})$$

where $\delta(\mathbf{r} - \mathbf{r}_0)$ is the 2D Dirac function. The above two equations are the lattice version of Eqs. (A1), (A2). The linear nature of oscillators suggests the analytical solution of $\mathbf{u}(\mathbf{r}_{i\alpha})$ with \mathbf{E} field. Suppose \mathbf{u} can be expanded as

$$\mathbf{u}(\mathbf{r}_{i\alpha}) = \sum_a \frac{1}{\sqrt{M_{\alpha}}} e^{i\mathbf{q}\cdot\mathbf{r}_{i\alpha}-i\omega t} \mathbf{e}_{\alpha,a}(\mathbf{q}) A_a(\mathbf{q}, \omega), \quad (\text{B3})$$

where $\mathbf{e}_a(\mathbf{q})$ is the displacement vector of the a -th eigen mode with frequency $\omega_{\mathbf{q}a}$, satisfying

$$\sum_{\beta\nu} D_{\alpha\mu,\beta\nu}(\mathbf{q}) e_{\beta\nu,a}(\mathbf{q}) = \omega_{\mathbf{q}a}^2 e_{\alpha\mu,a}(\mathbf{q}), \quad (\text{B4})$$

and the orthogonality

$$\sum_{\alpha\mu} e_{\alpha\mu,a}^*(\mathbf{q}) e_{\alpha\mu,a'}(\mathbf{q}) = \delta_{aa'}, \quad \sum_a e_{\alpha\mu,a}^*(\mathbf{q}) e_{\beta\nu,a}(\mathbf{q}) = \delta_{\alpha\beta} \delta_{\mu\nu}, \quad (\text{B5})$$

where the k -space dynamical matrix reads

$$D_{\alpha,\beta}(\mathbf{q}) = \sum_j \frac{\Phi_{\alpha,\beta}(\mathbf{r}_{i\alpha} - \mathbf{r}_{j\beta})}{\sqrt{M_\alpha M_\beta}} e^{i\mathbf{q}\cdot(\mathbf{r}_{j\beta} - \mathbf{r}_{i\alpha})}. \quad (\text{B6})$$

The target is to solve $A_a(\mathbf{q}, \omega)$. Plugging Eq. (B3) into Eq. (B1), we get

$$-\omega^2 \sum_a e_{\alpha\mu,a}(\mathbf{q}) A_a(\mathbf{q}, \omega) + \sum_{a\beta\nu} D_{\alpha\mu,\beta\nu}(\mathbf{q}) e_{\beta\nu,a}(\mathbf{q}) A_a(\mathbf{q}, \omega) - \frac{Z_\alpha e}{\sqrt{M_\alpha}} E_{\mathbf{q},\mu} = 0. \quad (\text{B7})$$

Then using Eqs. (B4), (B5), we get [recall that \mathbf{E}_t is the in-plane part of $\mathbf{E}(z=0)$]

$$(\omega_{qa}^2 - \omega^2) A_a(\mathbf{q}, \omega) = e \mathbf{S}_a^*(\mathbf{q}) \cdot \mathbf{E}_{\mathbf{q},t}, \quad (\text{B8})$$

where we have defined the S matrix

$$\mathbf{S}_a(\mathbf{q}) = \sum_\alpha \frac{Z_\alpha \mathbf{e}_{\alpha,a}(\mathbf{q})}{\sqrt{M_\alpha}}. \quad (\text{B9})$$

When $\omega \neq \omega_0$ (which is guaranteed in numerics by introducing a tiny linewidth $\omega + i\delta$), we can solve $A_a(\mathbf{q}, \omega)$ and plug it into Eq. (B3) to obtain \mathbf{u} .

To apply macroscopic Maxwell's equations, we need to abstract the continuous field $\mathbf{P}(\mathbf{r})$ from the lattice version Eq. (C4). This process is done by writing Eq. (C4) into Fourier series $\mathbf{P}_{\mathbf{q}+\mathbf{b}}$ (\mathbf{b} spans the reciprocal lattice) [7], but retain only the leading term with $\mathbf{b} = \mathbf{0}$ ($\mathbf{b} \neq \mathbf{0}$ terms are redundant because they detail the information within atomic unit cell, and are thus in-responsible for the long-wavelength physics)

$$\mathbf{P}(\mathbf{r}) = \sum_{\mathbf{b}} \mathbf{P}_{\mathbf{q}+\mathbf{b}}(\omega) e^{i(\mathbf{q}+\mathbf{b})\cdot\mathbf{r} - i\omega t} \rightarrow \mathbf{P}(\mathbf{r}) = \mathbf{P}_{\mathbf{q}}(\omega) e^{i\mathbf{q}\cdot\mathbf{r} - i\omega t}. \quad (\text{B10})$$

Then $\mathbf{P}_{\mathbf{q}}(\omega)$ can be calculated as

$$\mathbf{P}_{\mathbf{q}}(\omega) = \frac{1}{N_{\text{tot}}\Omega_0} \int d^2\mathbf{r} \mathbf{P}(\mathbf{r}) e^{-i\mathbf{q}\cdot\mathbf{r} + i\omega t} = \frac{1}{N_{\text{tot}}\Omega_0} \sum_{i\alpha} Z_\alpha e \mathbf{u}(\mathbf{r}_{i\alpha}) e^{-i\mathbf{q}\cdot\mathbf{r}_{i\alpha} + i\omega t} = \frac{e}{\Omega_0} \sum_a \mathbf{S}_a(\mathbf{q}) A_a(\mathbf{q}, \omega), \quad (\text{B11})$$

where Ω_0 is the area of atomic unit cell, N_{tot} is the total number of unit cells. Using Eq. (B8), we obtain

$$P_{\mathbf{q},\mu}(\omega) = \varepsilon_0 \sum_\nu \Pi_{\mu\nu}(\mathbf{q}, \omega) E_{\mathbf{q},\nu}(\omega), \quad (\text{B12})$$

where the in-plane susceptibility is a 2 by 2 matrix,

$$\Pi_{\mu\nu}(\mathbf{q}, \omega) = \frac{e^2}{\varepsilon_0 \Omega_0} \sum_a \frac{[\mathbf{S}_a(\mathbf{q})]_\mu [\mathbf{S}_a^*(\mathbf{q})]_\nu}{\omega_{qa}^2 - \omega^2}. \quad (\text{B13})$$

Actually this result is also correct in quantum case. By treating lattice dynamics as bosons, we will rederive it for moiré systems using the quantum linear response theory in Sec. E1. All the derivations of PhP conditions follow exactly the same procedure as in Secs. A3, A4, A5, since the macroscopic response function has already been obtained.

2. Relation to the macroscopic theory

Now it is time to relate the lattice model to the macroscopic model introduced in Sec. A1. We still focus on the moiré-less case. In the long-wavelength limit $|\mathbf{q}| \sim \omega_0/c$, the response function is almost isotropic and dispersionless, i.e.,

$$\Pi_{\mu\nu}(\mathbf{q}, \omega) \approx \delta_{\mu\nu} \Pi(\omega). \quad (\text{B14})$$

The nonzero contribution comes from the LO and TO modes (for acoustic modes, the polarization from opposite ions cancel due to in-phase oscillation), which gives the isotropic response

$$\Pi(\omega) = \frac{e^2}{\varepsilon_0 \Omega_0} \lim_{\mathbf{q} \rightarrow \mathbf{0}} \frac{|\mathbf{e}_q \cdot \mathbf{S}_{\text{LO}}(\mathbf{q})|^2}{\omega_{\mathbf{q},\text{LO}}^2 - \omega^2} = \frac{e^2}{\varepsilon_0 \Omega_0} \lim_{\mathbf{q} \rightarrow \mathbf{0}} \frac{|(\mathbf{e}_z \times \mathbf{e}_q) \cdot \mathbf{S}_{\text{TO}}(\mathbf{q})|^2}{\omega_{\mathbf{q},\text{TO}}^2 - \omega^2}. \quad (\text{B15})$$

Compared with Eq. (A11), we recognize

$$\omega_0 = \omega_{\mathbf{0},\text{LO}} = \omega_{\mathbf{0},\text{TO}}, \quad (\text{B16a})$$

$$T = \frac{e^2}{\varepsilon_0 \Omega_0} \lim_{\mathbf{q} \rightarrow \mathbf{0}} [\mathbf{e}_q \cdot \mathbf{S}_{\text{LO}}(\mathbf{q})]^2 = \frac{e^2}{\varepsilon_0 \Omega_0} \lim_{\mathbf{q} \rightarrow \mathbf{0}} [(\mathbf{e}_z \times \mathbf{e}_q) \cdot \mathbf{S}_{\text{TO}}(\mathbf{q})]^2. \quad (\text{B16b})$$

Substituting the above expressions into the static LO dispersion Eq. (A13), we obtain the LO-TO splitting (the so-called non-analytical correction) exactly the same as that in Ref. [10]:

$$\omega^2(\mathbf{q}) - \omega_0^2 = V(\mathbf{q}) \frac{q^2}{\Omega_0} |\mathbf{e}_q \cdot \mathbf{S}_{\text{LO}}(\mathbf{q})|_{\mathbf{q} \rightarrow \mathbf{0}}^2, \quad (\text{B17})$$

with the 2D Coulomb interaction $V(\mathbf{q}) = e^2/(2\varepsilon_0 \varepsilon q)$. The screening term is missing here because we have used the zero-thickness approximation from beginning [56]. From now on, for simplicity we focus on the monolayer hBN system. At $\mathbf{q} \approx \mathbf{0}$, for hBN the LO and TO phonons' eigen displacement can be obtained using the invariance of the center of mass: $M_N \mathbf{u}_N + M_B \mathbf{u}_B \propto \sqrt{M_N} \mathbf{e}_N + \sqrt{M_B} \mathbf{e}_B = 0$, so

$$\begin{aligned} \mathbf{e}_{\text{LO}}(\mathbf{q}) &= [\mathbf{e}_{N,\text{LO}}(\mathbf{q}), \mathbf{e}_{B,\text{LO}}(\mathbf{q})] \approx \left(\sqrt{\frac{M_B}{M_N + M_B}} \mathbf{e}_q, -\sqrt{\frac{M_N}{M_N + M_B}} \mathbf{e}_q \right)^T, \\ \mathbf{e}_{\text{TO}}(\mathbf{q}) &= [\mathbf{e}_{N,\text{TO}}(\mathbf{q}), \mathbf{e}_{B,\text{TO}}(\mathbf{q})] \approx \left(\sqrt{\frac{M_B}{M_N + M_B}} \mathbf{e}_z \times \mathbf{e}_q, -\sqrt{\frac{M_N}{M_N + M_B}} \mathbf{e}_z \times \mathbf{e}_q \right)^T. \end{aligned} \quad (\text{B18})$$

At $\mathbf{q} = \mathbf{0}$, $\mathbf{e}_q = \mathbf{q}/|q|$ is ill-defined, but we can fix $\mathbf{e}_0 = \mathbf{e}_x$, $\mathbf{e}_z \times \mathbf{e}_0 = \mathbf{e}_y$, i.e.,

$$\mathbf{e}_{\text{LO}}(\mathbf{0}) = \left(\sqrt{\frac{M_B}{M_N + M_B}} \mathbf{e}_x, -\sqrt{\frac{M_N}{M_N + M_B}} \mathbf{e}_x \right)^T, \quad \mathbf{e}_{\text{TO}}(\mathbf{0}) = \left(\sqrt{\frac{M_B}{M_N + M_B}} \mathbf{e}_y, -\sqrt{\frac{M_N}{M_N + M_B}} \mathbf{e}_y \right)^T. \quad (\text{B19})$$

For monolayer hBN, the T parameter can then be analytically derived as

$$\lim_{\mathbf{q} \rightarrow \mathbf{0}} \mathbf{e}_q \cdot \mathbf{S}_{\text{LO}}(\mathbf{q}) = \lim_{\mathbf{q} \rightarrow \mathbf{0}} (\mathbf{e}_z \times \mathbf{e}_q) \cdot \mathbf{S}_{\text{TO}}(\mathbf{q}) = \frac{Z_N}{\sqrt{M_N}} \sqrt{\frac{M_B}{M_N + M_B}} - \frac{Z_B}{\sqrt{M_B}} \sqrt{\frac{M_N}{M_N + M_B}}, \quad (\text{B20})$$

$$T = \frac{e^2}{\varepsilon_0 \Omega_0} \frac{M_N M_B}{M_N + M_B} \left(\frac{Z_N}{M_N} - \frac{Z_B}{M_B} \right)^2 = 3.842 \times 10^{19} \text{ m/s}^2. \quad (\text{B21})$$

Using $\omega_0 \approx 2\pi \times 49.4463$ THz, we get $T/(2\omega_0 c) \approx 2.06 \times 10^{-4}$, which is used to plot Fig. 1(b) in the main text. For the bilayer hBN without moiré potential (i.e., with no twist), T is doubled. Further, the macroscopic \mathbf{W} field is related to the lattice dynamics through

$$\mathbf{W}(\mathbf{r}, t) = \frac{1}{\sqrt{\Omega_0}} \sqrt{\frac{M_N M_B}{M_N + M_B}} [\mathbf{u}_N(\mathbf{r}, t) - \mathbf{u}_B(\mathbf{r}, t)] \propto \frac{1}{\sqrt{\Omega_0}} \sqrt{\frac{M_N M_B}{M_N + M_B}} \left[\frac{\mathbf{e}_N(\mathbf{q})}{\sqrt{M_N}} - \frac{\mathbf{e}_B(\mathbf{q})}{M_B} \right] e^{i\mathbf{q} \cdot \mathbf{r} - i\omega t}, \quad (\text{B22})$$

where $\mathbf{u}_\alpha(\mathbf{r}, t)$ is the continuum version [similar to Eq. (B10)] of the displacement field for sublattice α .

We now derive the continuum Huang's equations Eqs. (A1), (A2). The key point is, under the electric field, the optically active displacement field can be expanded using the field-free iLO/iTO modes [Eq. (B3)], i.e.,

$$\mathbf{u}(\mathbf{r}_{i\alpha}) = \frac{e^{i\mathbf{q} \cdot \mathbf{r}_{i\alpha}}}{\sqrt{M_\alpha}} (\mathbf{e}_{\alpha,\text{LO}}(\mathbf{q}), \mathbf{e}_{\alpha,\text{TO}}(\mathbf{q})) \begin{pmatrix} A_{\text{LO}} \\ A_{\text{TO}} \end{pmatrix}. \quad (\text{B23})$$

Notice that we have absorbed the time dependence into $A_{\text{LO/TO}}$. Then from Eq. (B7) we know

$$\begin{aligned} \frac{Z_\alpha e}{M_\alpha} \mathbf{E}_\mathbf{q} e^{i\mathbf{q}\cdot\mathbf{r}_{i\alpha} - i\omega t} &= \sum_a \frac{e^{i\mathbf{q}\cdot\mathbf{r}_{i\alpha}}}{\sqrt{M_\alpha}} \mathbf{e}_{\alpha,a}(\mathbf{q}) \ddot{A}_a + \sum_a \omega_{\mathbf{q}a}^2 \frac{e^{i\mathbf{q}\cdot\mathbf{r}_{i\alpha}}}{\sqrt{M_\alpha}} \mathbf{e}_{\alpha,a}(\mathbf{q}) A_a \\ &\approx \sum_a \frac{e^{i\mathbf{q}\cdot\mathbf{r}_{i\alpha}}}{\sqrt{M_\alpha}} \mathbf{e}_{\alpha,a}(\mathbf{q}) \ddot{A}_a + \omega_0^2 \sum_a \frac{e^{i\mathbf{q}\cdot\mathbf{r}_{i\alpha}}}{\sqrt{M_\alpha}} \mathbf{e}_{\alpha,a}(\mathbf{q}) A_a \\ &= \ddot{\mathbf{u}}(\mathbf{r}_{i\alpha}) + \omega_0^2 \mathbf{u}(\mathbf{r}_{i\alpha}), \end{aligned} \quad (\text{B24})$$

where we have adopted the Einstein approximation: $\omega_{\mathbf{q}a} = \omega_0$ (ω_0 is the degenerate eigen frequency of iLO/iTO modes at $\mathbf{q} = \mathbf{0}$) in the second line. The continuum version of the above equation of motion is simply $\ddot{\mathbf{u}}_\alpha(\mathbf{r}, t) = -\omega_0^2 \mathbf{u}_\alpha(\mathbf{r}, t) + (Z_\alpha e/M_\alpha) \mathbf{E}_t(\mathbf{r}, t)$. Then using the relation Eq. (B22) we get Eq. (A1)

$$\ddot{\mathbf{W}}(\mathbf{r}, t) = -\omega_0^2 \mathbf{W}(\mathbf{r}, t) + \frac{e}{\sqrt{\Omega_0}} \sqrt{\frac{M_N M_B}{M_N + M_B}} \left(\frac{Z_N}{M_N} - \frac{Z_B}{M_B} \right) \mathbf{E}_t(\mathbf{r}, t). \quad (\text{B25})$$

The relationship Eq. (A2) is easily obtained through the continuum version of Eq. (B2)

$$\mathbf{P}(\mathbf{r}, t) = \frac{1}{\Omega_0} \sum_\alpha Z_\alpha e \mathbf{u}_\alpha(\mathbf{r}, t) = \frac{Z_N e}{\Omega_0} (\mathbf{u}_N - \mathbf{u}_B) = \frac{Z_N e}{\sqrt{\Omega_0}} \sqrt{\frac{1}{M_N} + \frac{1}{M_B}} \mathbf{W}(\mathbf{r}, t). \quad (\text{B26})$$

So we see the microscopic expressions for γ_{12} , γ_{21} appearing in Eqs. (A1), (A2) are

$$\gamma_{12} = \frac{e}{\sqrt{\Omega_0}} \sqrt{\frac{M_N M_B}{M_N + M_B}} \left(\frac{Z_N}{M_N} - \frac{Z_B}{M_B} \right) = \frac{Z_N e}{\sqrt{\Omega_0}} \sqrt{\frac{1}{M_N} + \frac{1}{M_B}} = \gamma_{21}, \quad (\text{B27})$$

and $\gamma_{12}^2 = \gamma_{21}^2 = \varepsilon_0 T$ is recovered. We notice that in deriving the continuum theory, the \mathbf{q} -dependence in the phonon level has been abandoned, which is an excellent approximation since the optical region $q \sim q_0 = \omega_0/c$ is four to five orders smaller than the Brillouin zone size $1/a_0$. In other words, the \mathbf{q} -dispersion of PhP comes almost completely from light. We notice also that, in the moiré case when Eq. (C1) is satisfied, we can still abandon the $\bar{\mathbf{q}}$ -dependence. But it is necessary to retain the \mathbf{Q} -dependence of $\omega_{\bar{\mathbf{q}}+\mathbf{Q},b}$ (and dynamical matrix): $\omega_{\bar{\mathbf{q}}+\mathbf{Q},b} \approx \omega_{\mathbf{Q},b}$. It is such splitting of $\omega_{\mathbf{Q},b}$ that gives rise to the multiple branches of moiré PhP.

3. Force constant of monolayer hBN

Here we list the lattice model we used for the monolayer hBN. The short-ranged elastic force constants (FC) $\Phi_{\alpha,\beta}(\mathbf{r}_{i\alpha} - \mathbf{r}_{j\beta})$ are used to generate the bare phonon dispersion and eigen displacement vectors. Moreover, this monolayer model provides the moiré-less basis in the continuum model we will derive in Secs. D2 and D3.

The monolayer hBN is a hexagonal lattice with lattice constant $a_0 = 2.504 \text{ \AA}$. The Bravais lattice vectors are $\mathbf{a}_1 = a_0(1/2, \sqrt{3}/2)$, $\mathbf{a}_2 = a_0(-1/2, \sqrt{3}/2)$. The nitride (N) and boron (B) atoms are located at $\boldsymbol{\tau}_N = -\boldsymbol{\tau}_B = (\mathbf{a}_1 + \mathbf{a}_2)/3 = (a_0/\sqrt{3})\mathbf{e}_y$ near the origin. The lattice has the C_{3z} , C_{2y} and M_z symmetries. Notice that M_z results in the decoupling of in-plane and out-of-plane phonons of hBN monolayer, so we can consider only the in-plane parts. For simplicity we retain only the onsite, nearest-neighboring (n.n.), and next-nearest neighboring (n.n.n.) FCs. Each N (B) atom has 3 n.n. B (N) atoms, denoted by 3 relative vectors $(\mathbf{r}_{iN} - \mathbf{r}_{jB})_{\text{n.n.}} \in \{\boldsymbol{\delta}_1^0, \boldsymbol{\delta}_2^0, \boldsymbol{\delta}_3^0\}$, where $\boldsymbol{\delta}_1^0 = -(a_0/\sqrt{3})\mathbf{e}_y$, and $\boldsymbol{\delta}_2^0 = C_{3z}\boldsymbol{\delta}_1^0$, $\boldsymbol{\delta}_3^0 = C_{3z}^2\boldsymbol{\delta}_1^0$. The n.n. FCs are (in x, y basis)

$$\Phi_{N,B}(\boldsymbol{\delta}_1^0) = \begin{pmatrix} t_{xx}^0 & \\ & t_{yy}^0 \end{pmatrix}, \quad \Phi_{N,B}(\boldsymbol{\delta}_2^0) = C_{3z} \Phi_{N,B}(\boldsymbol{\delta}_1^0) C_{3z}^{-1}, \quad \Phi_{N,B}(\boldsymbol{\delta}_3^0) = C_{3z}^{-1} \Phi_{N,B}(\boldsymbol{\delta}_1^0) C_{3z}. \quad (\text{B28})$$

The other n.n. FCs are obtained through $\Phi_{B,N}(-\boldsymbol{\delta}_j^0) = \Phi_{N,B}^T(\boldsymbol{\delta}_j^0)$ for $j = 1, 2, 3$ (T is the transpose). Each N (B) atom has 6 n.n.n. N (B) atoms, denoted by 6 relative vectors $(\mathbf{r}_{iN(B)} - \mathbf{r}_{jN(B)})_{\text{n.n.n.}} \in \{\boldsymbol{\delta}_j^1 (j = 1, 2, \dots, 6)\}$, where $\boldsymbol{\delta}_1^1 = a_0\mathbf{e}_x$, and $\boldsymbol{\delta}_j^1 = C_{6z}^{j-1}\boldsymbol{\delta}_1^1$. The n.n.n. FCs are

$$\begin{aligned} \Phi_{N,N}(\boldsymbol{\delta}_1^1) &= \begin{pmatrix} t_{xx}^1 & t_{xy}^1 \\ -t_{xy}^1 & t_{yy}^1 \end{pmatrix}, \quad \Phi_{N,N}(\boldsymbol{\delta}_3^1) = C_{3z} \Phi_{N,N}(\boldsymbol{\delta}_1^1) C_{3z}^{-1}, \quad \Phi_{N,N}(\boldsymbol{\delta}_6^1) = C_{3z}^{-1} \Phi_{N,N}(\boldsymbol{\delta}_1^1) C_{3z}, \\ \Phi_{N,N}(\boldsymbol{\delta}_2^1) &= \Phi_{N,N}^T(\boldsymbol{\delta}_5^1), \quad \Phi_{N,N}(\boldsymbol{\delta}_4^1) = \Phi_{N,N}^T(\boldsymbol{\delta}_1^1), \quad \Phi_{N,N}(\boldsymbol{\delta}_6^1) = \Phi_{N,N}^T(\boldsymbol{\delta}_1^1). \end{aligned} \quad (\text{B29})$$

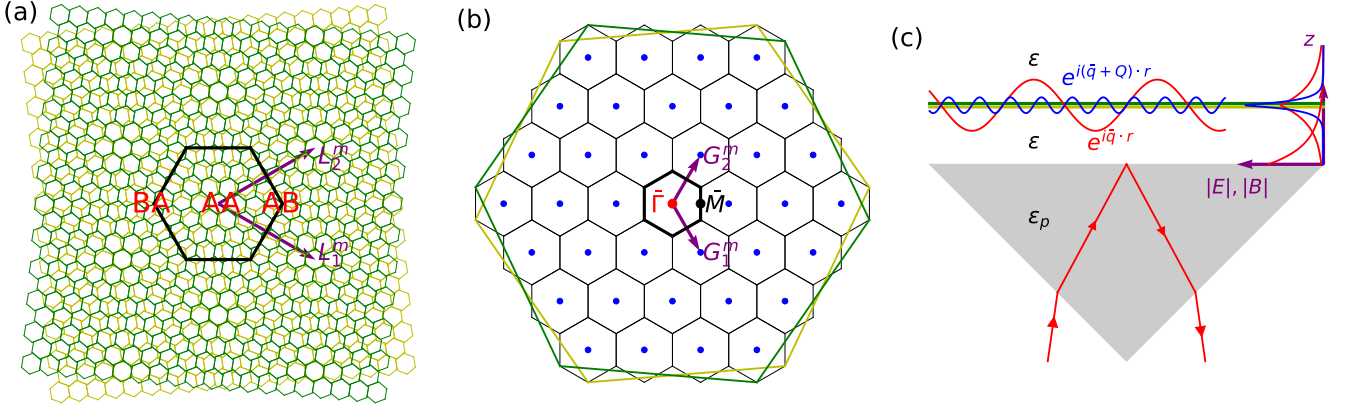


FIG. 5. (a) The lattice setup of a twisted bilayer hexagonal lattice. The moiré superlattice is characterized by the supercell (black) and the translation vectors $L_{1,2}^m$. Different stacking area like AA, AB/BA are also formed. (b) The formation of the corresponding mBZ (bold black) and reciprocal basis vectors $G_{1,2}^m$. The red dot denotes $\bar{\Gamma} = \mathbf{0}$. Blue dots denote all other $\mathbf{Q} \neq \mathbf{0}$ points, which will fold into $\bar{\Gamma}$ point in the mBZ. For visual convenience, in (a) and (b) we plot for the $N_a = 37$, $\theta = 9.43^\circ$ case. (c) The Otto configuration to excite moiré PhP in far-field technique. A prism (gray) is used to generate long-wavelength attenuate incident light (red arrows), which can excite phonons and EM components with shorter wavelengths ($\mathbf{Q} \neq \mathbf{0}$, blue).

The FCs among B atoms are $\Phi_{B,B}(\delta_j^1) = \Phi_{N,N}^T(\delta_j^1)$. Notice that $\Phi_{B,B}$ and $\Phi_{N,N}$ are actually independent, i.e., they are not related by any symmetry. In our present simple model they are set dependent, which is also supported by MD simulations. The onsite FCs are obtained through the sum rule

$$\Phi_{N,N}(\mathbf{0}) = -\sum_{j=1}^3 \Phi_{N,B}(\delta_j^0) - \sum_{j=1}^6 \Phi_{N,N}(\delta_j^1), \quad \Phi_{B,B}(\mathbf{0}) = -\sum_{j=1}^3 \Phi_{B,N}(\delta_j^0) - \sum_{j=1}^6 \Phi_{B,B}(\delta_j^1). \quad (\text{B30})$$

Using these FCs, the dynamical matrix can be easily calculated as

$$D_{\alpha,\alpha}(\mathbf{q}) = \frac{1}{M_\alpha} \left[\Phi_{\alpha,\alpha}(\mathbf{0}) + \sum_{j=1}^6 \Phi_{\alpha,\alpha}(\delta_j^1) e^{-i\mathbf{q}\cdot\delta_j^1} \right], \quad \alpha = N, B, \quad (\text{B31})$$

$$D_{N,B}(\mathbf{q}) = \frac{1}{\sqrt{M_N M_B}} \sum_{j=1}^3 \Phi_{N,B}(\delta_j^0) e^{-i\mathbf{q}\cdot\delta_j^0}, \quad D_{B,N}(\mathbf{q}) = D_{N,B}^\dagger(\mathbf{q}).$$

where the mass of atoms are $M_N = 14.0067$ amu, $M_B = 10.811$ amu. The numerical values of the constants above are found to be (unit: $\text{eV} \cdot \text{\AA}^{-2}$)

$$t_{xx}^0 = -6.8033, \quad t_{yy}^0 = -33.8892, \quad t_{xx}^1 = -1.6156, \quad t_{xy}^1 = -1.4759, \quad t_{yy}^1 = 0.2661, \quad (\text{B32})$$

obtain by MD simulations (Sec. F).

If the lattice setup is rotated anti-clockwisely by $\theta_l = (-1)^l \theta / 2$ ($l = 1, 2$ denote the two layers in twisted bilayer hBN), the intra-layer dynamical matrix $D_{l\alpha,l\beta}^0$ will be rotated from Eq. (B31) correspondingly through

$$D_{l\alpha,l\beta}^0(\mathbf{q}) = C_{\theta_l} D_{\alpha,\beta}(C_{\theta_l}^{-1} \mathbf{q}) C_{\theta_l}^{-1}, \quad C_{\theta_l} = \begin{pmatrix} \cos \theta_l & -\sin \theta_l \\ \sin \theta_l & \cos \theta_l \end{pmatrix}. \quad (\text{B33})$$

Appendix C: Lattice model of 2D PhP in moiré polar systems

1. Equation of motion and polarization in moiré superlattice

Moiré systems have a huge sublattice degree of freedom. Here we study modes of moiré materials with atomic thickness (not the setup in Ref. [19]). We use the notations defined in Refs. [35, 36]. Suppose each moiré supercell

contains N_a atomic unit cells, i.e., the supercell area Ω_m and atomic cell area Ω_0 are related by $\Omega_m = N_a\Omega_0$. Each atom's equilibrium position can be labeled as $\mathbf{r}_{I\alpha} = \mathbf{L}_I + \mathbf{R}_i + \boldsymbol{\tau}_\alpha$, where \mathbf{L}_I is the moiré Bravais lattice vector, \mathbf{R}_i (be careful, $i = 1, \dots, N_a$ takes finite positions now within a supercell) denotes the atomic Bravais lattice module the moiré lattice, and $\boldsymbol{\tau}_\alpha$ is the ion position within each atomic cell. We use $\bar{\mathbf{q}}$ to denote wave vectors in the moiré Brillouin zone (mBZ), and \mathbf{Q} the moiré reciprocal basis vectors (within the atomic Brillouin zone (aBZ), thus totally we have N_a different \mathbf{Q} vectors [36]).

We are interested in the regime with length scale orders

$$a_0 \ll L_\theta \ll \frac{c}{\omega_0}, \quad (\text{C1})$$

where a_0, L_θ are atomic and supercell lengths, respectively, ω_0 is the optical phonon frequency. The moiré potential, here is the local force field $\Phi_{i\alpha, j\beta}$, couples different \mathbf{Q} components (with length scale L_θ) together. So we insert a multi-wavelength in-plane field at $z = 0$,

$$\mathbf{E}_t = \sum_{\mathbf{Q}} \mathbf{E}_{\bar{\mathbf{q}}+\mathbf{Q}, t} e^{i(\bar{\mathbf{q}}+\mathbf{Q}) \cdot \mathbf{r} - i\omega t}, \quad (\text{C2})$$

into the equation of motion of the ionic displacement \mathbf{u} ,

$$M_\alpha \ddot{u}_\mu(\mathbf{r}_{I\alpha}) + \sum_{Jj\beta\nu} \Phi_{i\alpha\mu, j\beta\nu}(\mathbf{r}_{I\alpha} - \mathbf{r}_{Jj\beta}) u_\nu(\mathbf{r}_{Jj\beta}) - \sum_{\mathbf{Q}} Z_\alpha e E_{\bar{\mathbf{q}}+\mathbf{Q}, \mu}(\omega) e^{i(\bar{\mathbf{q}}+\mathbf{Q}) \cdot \mathbf{r}_{I\alpha} - i\omega t} = 0. \quad (\text{C3})$$

The polarization density is similarly defined as

$$\mathbf{P}(\mathbf{r}) = \sum_{I\alpha} Z_\alpha e \mathbf{u}(\mathbf{r}_{I\alpha}) \delta(\mathbf{r} - \mathbf{r}_{I\alpha}). \quad (\text{C4})$$

Even in the present moiré case, the solution is still analytical, and the derivation is almost parallel to the moiré-less case. Suppose \mathbf{u} can be expanded as

$$\mathbf{u}(\mathbf{r}_{I\alpha}) = \sum_b \frac{1}{\sqrt{M_\alpha}} e^{i\bar{\mathbf{q}} \cdot \mathbf{r}_{I\alpha} - i\omega t} e_{i\alpha, b}(\bar{\mathbf{q}}) A_b(\bar{\mathbf{q}}, \omega), \quad (\text{C5})$$

where $e_b(\bar{\mathbf{q}})$ is the eigen vector corresponding to the b -th field-free mode with frequency $\omega_b(\bar{\mathbf{q}})$,

$$\sum_{j\beta\nu} D_{i\alpha\mu, j\beta\nu}(\bar{\mathbf{q}}) e_{j\beta\nu, b}(\bar{\mathbf{q}}) = \omega_b^2(\bar{\mathbf{q}}) e_{i\alpha\mu, b}(\bar{\mathbf{q}}), \quad (\text{C6})$$

and the moiré dynamical matrix reads

$$D_{i\alpha, j\beta}(\bar{\mathbf{q}}) = \sum_J \frac{\Phi_{i\alpha, j\beta}(\mathbf{L}_I - \mathbf{L}_J)}{\sqrt{M_\alpha M_\beta}} e^{i\bar{\mathbf{q}} \cdot (\mathbf{r}_{Jj\beta} - \mathbf{r}_{I\alpha})}. \quad (\text{C7})$$

The target is to solve $A_b(\bar{\mathbf{q}}, \omega)$. Plugging Eq. (C5) into Eq. (C3), and using the orthogonality

$$\sum_{i\alpha\mu} e_{i\alpha\mu, b}^*(\bar{\mathbf{q}}) e_{i\alpha\mu, b'}(\bar{\mathbf{q}}) = \delta_{bb'}, \quad \sum_b e_{i\alpha\mu, b}^*(\bar{\mathbf{q}}) e_{j\beta\nu, b}(\bar{\mathbf{q}}) = \delta_{ij} \delta_{\alpha\beta} \delta_{\mu\nu}, \quad (\text{C8})$$

we get

$$(\omega_{\bar{\mathbf{q}}b}^2 - \omega^2) A_b(\bar{\mathbf{q}}, \omega) = e \sum_{\mathbf{Q}} \mathbf{S}_{\mathbf{Q}b}^*(\bar{\mathbf{q}}) \cdot \mathbf{E}_{\bar{\mathbf{q}}+\mathbf{Q}, t}, \quad (\text{C9})$$

where the moiré S matrix has an additional \mathbf{Q} index,

$$\mathbf{S}_{\mathbf{Q}b}(\bar{\mathbf{q}}) = \sum_{i\alpha} \frac{Z_\alpha e_{i\alpha, b}(\bar{\mathbf{q}})}{\sqrt{M_\alpha}} e^{-i\mathbf{Q} \cdot (\mathbf{R}_i + \boldsymbol{\tau}_\alpha)}. \quad (\text{C10})$$

We now abstract the continuous field $\mathbf{P}(\mathbf{r})$ from Eq. (C4). Writing Eq. (C4) into Fourier series $\mathbf{P}_{\bar{\mathbf{q}}+\mathbf{Q}}$, but this time we retain some leading terms, i.e., components with $|\mathbf{Q}| \ll 2\pi/a_0$ (a_0 is the atomic cell length. Higher-order terms are redundant because they detail the information within atomic unit cell)

$$\mathbf{P}(\mathbf{r}) = \sum_{\mathbf{Q}} \mathbf{P}_{\bar{\mathbf{q}}+\mathbf{Q}}(\omega) e^{i(\bar{\mathbf{q}}+\mathbf{Q})\cdot\mathbf{r}-i\omega t}. \quad (\text{C11})$$

Notice that $\mathbf{Q} \neq \mathbf{0}$ terms are necessary to retain here because they reflect the dipole fluctuation in moiré length scales. The component $\mathbf{P}_{\bar{\mathbf{q}}+\mathbf{Q}}(\omega)$ is calculated as

$$\mathbf{P}_{\bar{\mathbf{q}}+\mathbf{Q}} = \frac{1}{N_m \Omega_m} \sum_{Ii\alpha} Z_\alpha e \mathbf{u}(\mathbf{r}_{Ii\alpha}) e^{-i(\bar{\mathbf{q}}+\mathbf{Q})\cdot\mathbf{r}_{Ii\alpha}+i\omega t} = \frac{e}{\Omega_m} \sum_b \mathbf{S}_{\mathbf{Q}b}(\bar{\mathbf{q}}) A_b(\bar{\mathbf{q}}, \omega). \quad (\text{C12})$$

Using Eq. (C9), we can write down

$$P_{\bar{\mathbf{q}}+\mathbf{Q},\mu}(\omega) = \varepsilon_0 \sum_{\mathbf{Q}'\nu} \Pi_{\mu\nu}^{\mathbf{Q}\mathbf{Q}'}(\bar{\mathbf{q}}, \omega) E_{\bar{\mathbf{q}}+\mathbf{Q}',\nu}, \quad (\text{C13})$$

where the susceptibility now is a tensor with index \mathbf{Q} ,

$$\Pi_{\mu\nu}^{\mathbf{Q}\mathbf{Q}'}(\bar{\mathbf{q}}, \omega) = \frac{e^2}{\varepsilon_0 \Omega_m} \sum_b \frac{[\mathbf{S}_{\mathbf{Q}b}(\bar{\mathbf{q}})]_\mu [\mathbf{S}_{\mathbf{Q}'b}^*(\bar{\mathbf{q}})]_\nu}{\omega_{\bar{\mathbf{q}}b}^2 - \omega^2}. \quad (\text{C14})$$

It will be convenient to decompose the in-plane fields into directions along and perpendicular to $\bar{\mathbf{q}} + \mathbf{Q}$,

$$\mathbf{E}_{\bar{\mathbf{q}}+\mathbf{Q},t} = E_{\bar{\mathbf{q}}+\mathbf{Q},\parallel} \mathbf{e}_{\bar{\mathbf{q}}+\mathbf{Q},\parallel} + E_{\bar{\mathbf{q}}+\mathbf{Q},\perp} \mathbf{e}_{\bar{\mathbf{q}}+\mathbf{Q},\perp}, \quad (\text{C15})$$

where

$$\mathbf{e}_{\bar{\mathbf{q}}+\mathbf{Q},\parallel} = (\bar{\mathbf{q}} + \mathbf{Q})/|\bar{\mathbf{q}} + \mathbf{Q}|, \quad \mathbf{e}_{\bar{\mathbf{q}}+\mathbf{Q},\perp} = \mathbf{e}_z \times \mathbf{e}_{\bar{\mathbf{q}}+\mathbf{Q},\parallel}. \quad (\text{C16})$$

Correspondingly we can decompose $\Pi^{\mathbf{Q}\mathbf{Q}'}$ into $(\alpha, \beta = \parallel, \perp, \mu, \nu = x, y)$

$$\Pi_{\mu\nu}^{\mathbf{Q}\mathbf{Q}'}(\bar{\mathbf{q}}, \omega) = \sum_{\alpha\beta} \Pi_{\alpha\beta}^{\mathbf{Q}\mathbf{Q}'}(\bar{\mathbf{q}}, \omega) [\mathbf{e}_{\bar{\mathbf{q}}+\mathbf{Q},\alpha}]_\mu [\mathbf{e}_{\bar{\mathbf{q}}+\mathbf{Q}',\beta}]_\nu. \quad (\text{C17})$$

The moiré physics enter polaritons by providing the susceptibility $\Pi(\bar{\mathbf{q}}, \omega)$ with off-diagonal $\mathbf{Q} \neq \mathbf{Q}'$ terms. In real space this corresponds to the inhomogeneous optical response. If we turn off the moiré potential, phonons are simply folded from the moiré-less system. In other words, \mathbf{Q} is still a good quantum number, and the mode index $b = (\mathbf{Q}, a)$ where a is the atomic phonon branch index (for hBN, $a = 1, \dots, 6$). In this case Π becomes diagonal about \mathbf{Q} , and the diagonal term $\Pi^{\mathbf{Q}\mathbf{Q}}(\bar{\mathbf{q}}, \omega)$ reduces just to the moiré-less one with momentum $\bar{\mathbf{q}} + \mathbf{Q}$. See subsection E 4 for details.

2. Moiré polaritons

After the continuation of \mathbf{P} , the whole system of equations is completed by applying Maxwell's equations, using the method in Sec. A 5. The moiré material (assumed to have zero width) is placed at $z = 0$ and the tentative incidence comes from $z < 0$. Assume in general that the incident ($l = i, z < 0$), reflected ($l = r, z < 0$), and transmitted ($l = t, z > 0$) lights are

$$\begin{aligned} \mathbf{E}^i(\mathbf{r}, t) &= \sum_{\mathbf{Q}\alpha} E_{\bar{\mathbf{q}}+\mathbf{Q},\alpha}^i \mathbf{e}_{\bar{\mathbf{q}}+\mathbf{Q},\alpha} e^{i(\bar{\mathbf{q}}+\mathbf{Q})\cdot\mathbf{r}-\lambda_{\mathbf{Q}}z-i\omega t}, \\ \mathbf{E}^r(\mathbf{r}, t) &= \sum_{\mathbf{Q}\alpha} E_{\bar{\mathbf{q}}+\mathbf{Q},\alpha}^r \mathbf{e}_{\bar{\mathbf{q}}+\mathbf{Q},\alpha} e^{i(\bar{\mathbf{q}}+\mathbf{Q})\cdot\mathbf{r}+\lambda_{\mathbf{Q}}z-i\omega t}, \\ \mathbf{E}^t(\mathbf{r}, t) &= \sum_{\mathbf{Q}\alpha} E_{\bar{\mathbf{q}}+\mathbf{Q},\alpha}^t \mathbf{e}_{\bar{\mathbf{q}}+\mathbf{Q},\alpha} e^{i(\bar{\mathbf{q}}+\mathbf{Q})\cdot\mathbf{r}-\lambda_{\mathbf{Q}}z-i\omega t}, \end{aligned} \quad (\text{C18})$$

where α takes \parallel, \perp, z with $\mathbf{e}_{\bar{\mathbf{q}}+\mathbf{Q},z} = \mathbf{e}_z$, and

$$\lambda_{\mathbf{Q}} = \begin{cases} -i\sqrt{\varepsilon\frac{\omega^2}{c^2} - |\bar{\mathbf{q}} + \mathbf{Q}|^2}, & |\bar{\mathbf{q}} + \mathbf{Q}|^2 < \varepsilon\frac{\omega^2}{c^2} \\ \sqrt{|\bar{\mathbf{q}} + \mathbf{Q}|^2 - \varepsilon\frac{\omega^2}{c^2}}, & |\bar{\mathbf{q}} + \mathbf{Q}|^2 > \varepsilon\frac{\omega^2}{c^2} \end{cases}. \quad (\text{C19})$$

to fulfill Eq. (A9). The divergence law Eq. (A8) requires

$$E_{\bar{\mathbf{q}}+\mathbf{Q},z}^i = i\frac{|\bar{\mathbf{q}} + \mathbf{Q}|}{\lambda_{\mathbf{Q}}} E_{\bar{\mathbf{q}}+\mathbf{Q},\parallel}^i, \quad E_{\bar{\mathbf{q}}+\mathbf{Q},z}^r = -i\frac{|\bar{\mathbf{q}} + \mathbf{Q}|}{\lambda_{\mathbf{Q}}} E_{\bar{\mathbf{q}}+\mathbf{Q},\parallel}^r, \quad E_{\bar{\mathbf{q}}+\mathbf{Q},z}^t = i\frac{|\bar{\mathbf{q}} + \mathbf{Q}|}{\lambda_{\mathbf{Q}}} E_{\bar{\mathbf{q}}+\mathbf{Q},\parallel}^t. \quad (\text{C20})$$

Then the four BCs at the material surface give (written using electric fields)

$$\mathbf{E}_{\bar{\mathbf{q}}+\mathbf{Q},t}^t = \mathbf{E}_{\bar{\mathbf{q}}+\mathbf{Q},t}^i + \mathbf{E}_{\bar{\mathbf{q}}+\mathbf{Q},t}^r, \quad (\text{C21a})$$

$$E_{\bar{\mathbf{q}}+\mathbf{Q},z}^t - E_{\bar{\mathbf{q}}+\mathbf{Q},z}^i - E_{\bar{\mathbf{q}}+\mathbf{Q},z}^r = -\frac{i(\bar{\mathbf{q}} + \mathbf{Q}) \cdot \mathbf{P}_{\bar{\mathbf{q}}+\mathbf{Q}}}{\varepsilon_0 \varepsilon}, \quad (\text{C21b})$$

$$\lambda_{\mathbf{Q}}(\mathbf{E}_{\bar{\mathbf{q}}+\mathbf{Q},t}^i - \mathbf{E}_{\bar{\mathbf{q}}+\mathbf{Q},t}^r - \mathbf{E}_{\bar{\mathbf{q}}+\mathbf{Q},t}^t) - i(\bar{\mathbf{q}} + \mathbf{Q})(E_{\bar{\mathbf{q}}+\mathbf{Q},z}^t - E_{\bar{\mathbf{q}}+\mathbf{Q},z}^i - E_{\bar{\mathbf{q}}+\mathbf{Q},z}^r) = -\mu_0 \omega^2 \mathbf{P}_{\bar{\mathbf{q}}+\mathbf{Q}}, \quad (\text{C21c})$$

$$\mathbf{e}_z \cdot [(\bar{\mathbf{q}} + \mathbf{Q}) \times (\mathbf{E}_{\bar{\mathbf{q}}+\mathbf{Q},\perp}^t - \mathbf{E}_{\bar{\mathbf{q}}+\mathbf{Q},\perp}^i - \mathbf{E}_{\bar{\mathbf{q}}+\mathbf{Q},\perp}^r)] = 0. \quad (\text{C21d})$$

Similar to the case of toy model in Sec. A1, it is sufficient to consider only the 1st, 2nd, and the transverse part of the 3rd BCs (for each \mathbf{Q}). The 4th BC and the longitudinal part of the 3rd BC coincide with the 1st and 2nd BCs, respectively. Putting Eqs. (C13), (C20) into the above BCs, and using the 1st BC to eliminate \mathbf{E}_t^r , we may organize these BCs into a set of linear equations

$$\sum_{\mathbf{Q}'\beta} A_{\alpha\beta}^{\mathbf{Q}\mathbf{Q}'}(\bar{\mathbf{q}}, \omega) \mathbf{E}_{\bar{\mathbf{q}}+\mathbf{Q}',\beta}^t = \mathbf{E}_{\bar{\mathbf{q}}+\mathbf{Q},\alpha}^i, \quad (\text{C22})$$

with the matrix elements

$$A_{\parallel\parallel}^{\mathbf{Q}\mathbf{Q}'}(\bar{\mathbf{q}}, \omega) = \delta_{\mathbf{Q}\mathbf{Q}'} + \frac{\lambda_{\mathbf{Q}}}{2\varepsilon} \Pi_{\parallel\parallel}^{\mathbf{Q}\mathbf{Q}'}(\bar{\mathbf{q}}, \omega), \quad (\text{C23a})$$

$$A_{\parallel\perp}^{\mathbf{Q}\mathbf{Q}'}(\bar{\mathbf{q}}, \omega) = \frac{\lambda_{\mathbf{Q}}}{2\varepsilon} \Pi_{\parallel\perp}^{\mathbf{Q}\mathbf{Q}'}(\bar{\mathbf{q}}, \omega), \quad (\text{C23b})$$

$$A_{\perp\parallel}^{\mathbf{Q}\mathbf{Q}'}(\bar{\mathbf{q}}, \omega) = -\frac{1}{2\lambda_{\mathbf{Q}}} \frac{\omega^2}{c^2} \Pi_{\perp\parallel}^{\mathbf{Q}\mathbf{Q}'}(\bar{\mathbf{q}}, \omega), \quad (\text{C23c})$$

$$A_{\perp\perp}^{\mathbf{Q}\mathbf{Q}'}(\bar{\mathbf{q}}, \omega) = \delta_{\mathbf{Q}\mathbf{Q}'} - \frac{1}{2\lambda_{\mathbf{Q}}} \frac{\omega^2}{c^2} \Pi_{\perp\perp}^{\mathbf{Q}\mathbf{Q}'}(\bar{\mathbf{q}}, \omega). \quad (\text{C23d})$$

The above equation generalizes Eqs. (A27), (A28), and is the core result of this paper. From Eq. (C22) we can define the transmission and reflection tensors

$$T(\bar{\mathbf{q}}, \omega) = A^{-1}(\bar{\mathbf{q}}, \omega), \quad R(\bar{\mathbf{q}}, \omega) = A^{-1}(\bar{\mathbf{q}}, \omega) - I, \quad (\text{C24})$$

so that

$$\mathbf{E}_t^t = T(\bar{\mathbf{q}}, \omega) \mathbf{E}_t^i, \quad \mathbf{E}_t^r = R(\bar{\mathbf{q}}, \omega) \mathbf{E}_t^i, \quad (\text{C25})$$

written in the basis

$$\mathbf{E}_t^l = (E_{\bar{\mathbf{q}}+\mathbf{Q}_{1,\parallel}}^l, E_{\bar{\mathbf{q}}+\mathbf{Q}_{1,\perp}}^l, \dots, E_{\bar{\mathbf{q}}+\mathbf{Q}_{N_a,\perp}}^l)^T. \quad (\text{C26})$$

All the information about PhPs are contained in $A(\bar{\mathbf{q}}, \omega)$, e.g., the zeros of $\det(A)$ determines the polariton dispersion whose eigen EM fields read as the corresponding eigen vector. A salient feature of moiré PhP is that, as shown in Fig. 2(c) of the main text, due to the scattering of moiré potential, a long-wavelength incidence $\mathbf{E}_{\bar{\mathbf{q}}}^i$ can induce inhomogeneous responses $\mathbf{E}_{\bar{\mathbf{q}}+\mathbf{Q}}^{r,t}$ with $\mathbf{Q} \neq \mathbf{0}$, which never happens in moiré-less systems. Based on this property, we can focus on the long-wavelength incidence, which already captures information of moiré scattering and expels those with short wavelengths only. The effective transmission matrix is the $\mathbf{Q} = \mathbf{0}$ submatrix [31]

$$T_{\text{eff}}(\bar{\mathbf{q}}, \omega) = [A^{-1}(\bar{\mathbf{q}}, \omega)]^{00}. \quad (\text{C27})$$

The poles of the spectrum $\mathcal{L}(\bar{\mathbf{q}}, \omega) = -\text{Im}[\det[T_{\text{eff}}(\bar{\mathbf{q}}, \omega + i\delta)]]$ depicts the dispersion of moiré PhPs that can be excited by long-wavelength light. Since \mathcal{L} can change sign at some points, we instead plot the spectrum of $\ln(1 + |\mathcal{L}(\bar{\mathbf{q}}, \omega)|)$, whose poles are the same to \mathcal{L} , to visualize the dispersions of moiré PhP.

Appendix D: Macroscopic theory of moiré PhP

1. A toy model: coupled harmonic oscillators

Generally, with the presence of inhomogeneity, the system should be described by a set of coupled vibrational fields \mathbf{W}_b and electric fields \mathbf{E}_b . In the present case b labels just the different Fourier components \mathbf{Q} . More specifically, we use \mathbf{W}_0 and \mathbf{E}_0 to denote the usual long-wavelength fields (with momentum $\bar{\mathbf{q}} \approx \mathbf{0}$), while all other $b \neq 0$ terms correspond to high-momentum fields (with momentum $\bar{\mathbf{q}} + \mathbf{Q}$). The equation of motion and polarization density for the b -th component are

$$\ddot{\mathbf{W}}_b = - \sum_{b'} \mathcal{D}_{bb'} \mathbf{W}_{b'} + \gamma \mathbf{E}_b, \quad \mathbf{P}_b = \gamma \mathbf{W}_b, \quad (\text{D1})$$

where $\mathcal{D}_{bb'} = \mathcal{D}_{b'b}$ is the coupling constant among \mathbf{W}_b and $\mathbf{W}_{b'}$, γ is the charge coefficient. Notice that $\mathcal{D}_{bb} = \omega_b^2$ is the elastic eigen frequency. For simplicity these parameters are set real. The nontrivial inhomogeneity leads to $\mathcal{D}_{bb'} \neq 0$ when $b \neq b'$. We can decompose \mathbf{W}_b into the normal modes $\mathbf{W}_b = \sum_{b'} U_{bb'} \mathbf{w}_{b'}$ that diagonalizes the coupled system, where the orthogonal transformation matrix V satisfies

$$\sum_{b'} (\omega_b^2 \delta_{b''b'} - \mathcal{D}_{b''b'}) U_{b'b} = 0, \quad \sum_b U_{bb'} U_{bb''} = \sum_b U_{b'b} U_{b''b} = \delta_{b'b''}. \quad (\text{D2})$$

It can be easily checked that (suppose the system oscillates with frequency ω)

$$\ddot{\mathbf{w}}_b = -\omega_b^2 \mathbf{w}_b + \gamma \sum_{b'} U_{b'b} \mathbf{E}_{b'}, \quad \mathbf{P}_b = \gamma \sum_{b'} U_{bb'} \mathbf{w}_{b'} = \sum_{b''} \gamma^2 \frac{U_{bb''} U_{b''b'}}{\omega_{b''}^2 - \omega^2} \mathbf{E}_{b'}. \quad (\text{D3})$$

If we focus on the long-wavelength dispersion, we may neglect all short-wavelength fields \mathbf{w}_b , \mathbf{E}_b , and \mathbf{P}_b with $b \neq 0$. If so, after redefining $(\gamma U_{0b})^2 = \varepsilon_0 T_b$, we obtain the effective long-wavelength susceptibility

$$\Pi(\omega) = \Pi^{00}(\omega) = \sum_b \frac{T_b}{\omega_b^2 - \omega^2}, \quad (\text{D4})$$

which has multiple poles. By plugging this long-wavelength susceptibility into the TM mode equation Eq. (A19), we can qualitatively obtain the moiré PhP dispersion. In Fig. 6 we plot the TM dispersion by using such method and fitting the model of twisted MoTe₂. Notice that each pole ω_b has a specific strength T_b proportional to the scattering strength to that channel, and brings up a specific pair of TM and TE modes, if other poles do not exist. The TE modes are mainly lattice vibrations, contributing little to the PhP dispersion. The TM modes disperse linearly with slopes proportional to T_b starting from ω_b [Eq. (A13)]. So crossings happen between these branches with different slopes if they are not coupled. The whole frequency region is partitioned into a series of negative windows where $\Pi(\omega) < 0$ and positive windows where $\Pi(\omega) > 0$. Remembering the sign rule, the TM (TE) PhP lives separately in each negative (positive) window. This is true even when all the poles are taken into consideration. This results in the anti-crossings shown in Fig. 6 (b). The most dispersive (dominant) branch has largest T_b that carries most long-wavelength component. The moiré pattern of \mathbf{E} and \mathbf{W} is a byproduct: when ω approaches ω_b , the lattice oscillates exclusively in accordance with mode b , which generates a short-wavelength polarization, thus jointly inducing the moiré EM fields.

We observe that Ref. [32] adopts similar coupled oscillator model to explain the exciton polariton. Their two poles origins from the hetero structure. But here the multiple poles results from the umklapp scattering of the inhomogeneous moiré potential in the homobilayer. This is also the reason why these poles ω_b stay so close to each other. The stronger the moiré potential, the stronger splitting of ω_b could be observed. The PhP dispersion obtained using such coupled oscillator model (fitted with MoTe₂) is shown in Fig. 6, which captures the basic anti-crossing structures.

The coupled harmonic oscillator model presented in this subsection is only a toy model. It is only used to illustrate how the moiré potential brings multiple branches of PhP. We will render such model in next subsection, to make it more quantitative and accurate.

2. The continuum model for moiré phonon

A more accurate model should incorporate the anisotropy of TO and LO phonons at various moiré reciprocal momentum \mathbf{Q} . The macroscopic model for moiré PhP calls for a corresponding continuum model for optical moiré

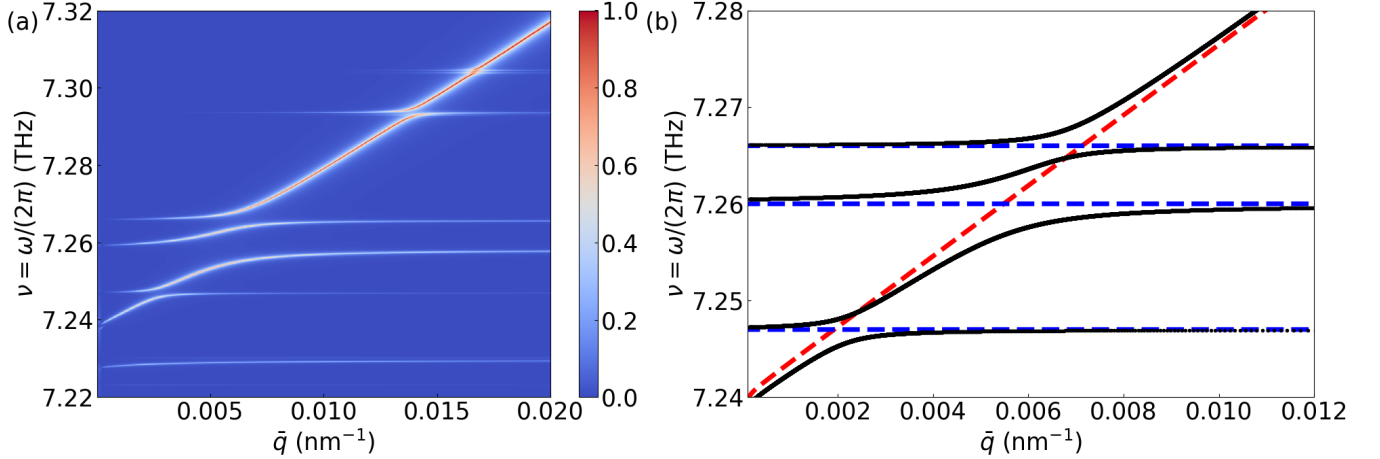


FIG. 6. (a) The long-wavelength PhP dispersion (along the $\bar{\Gamma} - \bar{M}$ line) of 3.89° twisted bilayer MoTe₂ near $\nu_0 \approx 7.2$ THz ($q_0 \approx 1.5 \times 10^{-4} \text{ nm}^{-1}$), obtained through the lattice model. Here we take $\delta/2\pi = 2 \times 10^{-4}$ THz. (b) The same PhP dispersion (black) obtained using the coupled oscillator model (TM mode). Here we take $\gamma_0^2/(2\pi)^4 = 3.7 \times 10^7 \text{ CV}^{-1}\text{s}^{-2}$, and for \mathcal{D} parameters [in the unit of $(2\pi\text{THz})^2$]: $\mathcal{D}_{00} = 7.240^2$, $\mathcal{D}_{11} = 7.247^2$, $\mathcal{D}_{22} = 7.260^2$, $\mathcal{D}_{33} = 7.266^2$, $\mathcal{D}_{01} = \mathcal{D}_{10} = 0.0204$, $\mathcal{D}_{02} = \mathcal{D}_{20} = 0.0456$, $\mathcal{D}_{03} = \mathcal{D}_{30} = 0.0236$, (all other parameters are set zero), obtained by fitting (a). For comparison, we also show the PhP dispersion (red dashed line) and non-dispersive phonon frequencies of high momentum \mathbf{Q} (blue dashed lines) in the decoupling case.

phonons (without long-wavelength electric field). The theoretical structure is quite similar to the Bistritzer-MacDonald (BM) model for electrons in the magic-angle twisted bilayer graphene [62], and is more conveniently obtained using the truncated plane wave (TAPW) method [35, 36].

The dynamical matrix (C7) has exactly the same form as the tight-binding Hamiltonian for electrons, thus suggesting the same mathematical and physical structure. The general idea of the TAPW method is to expand the eigenmodes of the moiré system using the monolayer “plane waves”, i.e.,

$$e_{i\alpha\mu,b}(\bar{\mathbf{k}}) = \sum_{\mathbf{Q}la} \frac{e^{i\mathbf{Q}\cdot(\mathbf{R}_i+\boldsymbol{\tau}_\alpha)}}{\sqrt{N_a}} e_{\alpha\mu,la}(\bar{\mathbf{q}}+\mathbf{Q}) U_{\mathbf{Q}la,b}(\bar{\mathbf{q}}), \quad (\text{D5})$$

where the vector $e_{la}(\mathbf{q})$ (a : branch, l : layer) satisfies the monolayer dynamical equation Eq. (B4) and orthogonality Eq. (B5). If we turn off the moiré potential, $U(\bar{\mathbf{q}})$ becomes diagonal and the phonons just reduce to those folded from the monolayer case without any hybridization (Sec. E4). We can expect that a small truncation of \mathbf{Q} vectors in the Γ valley (here we take $N_{\mathbf{Q}} = 61$) is sufficient to calculate the phonons there. Also we only want to focus on the iLO and iTO modes, so we simply limit the summation over a to these two branches. Therefore, the TAPW method reduces the dimension to $4N_{\mathbf{Q}}$. The U matrix satisfies

$$\sum_{\mathbf{Q}'l'a'} \mathcal{D}_{\mathbf{Q}la,\mathbf{Q}'l'a'}(\bar{\mathbf{q}}) U_{\mathbf{Q}'l'a',b}(\bar{\mathbf{q}}) = \omega_{\bar{\mathbf{q}}b}^2 U_{\mathbf{Q}la,b}(\bar{\mathbf{q}}), \quad (\text{D6})$$

where the transformed dynamical matrix is derived to be [35, 36]

$$\mathcal{D}_{\mathbf{Q}la,\mathbf{Q}'l'a'}(\bar{\mathbf{q}}) = \sum_{i\alpha\mu,j\beta\nu} e_{\alpha\mu,la}^*(\bar{\mathbf{q}}+\mathbf{Q}) \frac{e^{-i\mathbf{Q}\cdot(\mathbf{R}_i+\boldsymbol{\tau}_\alpha)}}{\sqrt{N_a}} D_{i\alpha\mu,j\beta\nu}(\bar{\mathbf{q}}) \frac{e^{i\mathbf{Q}'\cdot(\mathbf{R}_j+\boldsymbol{\tau}_\beta)}}{\sqrt{N_a}} e_{\beta\nu,l'a'}(\bar{\mathbf{q}}+\mathbf{Q}'). \quad (\text{D7})$$

The following target is to simplify $\mathcal{D}(\bar{\mathbf{q}})$. For convenience, we fix the direction of iLO/iTO basis at different $\bar{\mathbf{q}}+\mathbf{Q}$, and use the following basis at $\mathbf{q}=\mathbf{0}$ to replace $e_{\alpha,la}(\mathbf{q})$ [see Eq. (B19)]

$$\mathbf{e}_{lx} = \left(\sqrt{\frac{M_B}{M_N+M_B}}, 0, -\sqrt{\frac{M_N}{M_N+M_B}}, 0 \right)^T, \quad \mathbf{e}_{ly} = \left(0, \sqrt{\frac{M_B}{M_N+M_B}}, 0, -\sqrt{\frac{M_N}{M_N+M_B}} \right)^T. \quad (\text{D8})$$

This step itself is an approximation that assumes the Hilbert space spanned by iLO/iTO modes at $\bar{\mathbf{q}}+\mathbf{Q}$ is the same as the Γ point. But it greatly simplifies the calculation since it abandons the complex \mathbf{q} -dependence of $e_{la}(\mathbf{q})$ in the

$k \cdot p$ spirit. Correspondingly, we replace the index $a = \text{iLO, iTTO}$ by the index $A = x, y$, and the dynamical matrix in basis Eq. (D8) becomes

$$\mathcal{D}_{\mathbf{Q}l\mu, \mathbf{Q}'l'\nu}(\bar{\mathbf{q}}) = \sum_{i\alpha, j\beta} \frac{e^{-i\mathbf{Q} \cdot (\mathbf{R}_i + \boldsymbol{\tau}_\alpha)}}{\sqrt{N_a}} e_{\alpha, l\mu}^* D_{i\alpha, j\beta}(\bar{\mathbf{q}}) e_{\beta, l'\nu} \frac{e^{i\mathbf{Q}' \cdot (\mathbf{R}_j + \boldsymbol{\tau}_\beta)}}{\sqrt{N_a}}. \quad (\text{D9})$$

Then, the intralayer $l = l'$ terms with $\mathbf{Q} = \mathbf{Q}'$ are easy to deal with. We can simply diagonalize the monolayer dynamical matrix at $\bar{\mathbf{q}} + \mathbf{Q}$ [i.e., $D_{l\alpha, l\beta}^0(\bar{\mathbf{q}} + \mathbf{Q})$ defined in Eq. (B33)], and use the monolayer iLO/iTO frequencies (denoted by $\omega_{\bar{\mathbf{q}}+\mathbf{Q}, la}^0$) to write

$$\mathcal{D}_{\mathbf{Q}l\mu, \mathbf{Q}l\nu}^0(\bar{\mathbf{q}}) = \sum_a^{\text{iLO, iTTO}} (\omega_{\bar{\mathbf{q}}+\mathbf{Q}, la}^0)^2 e_{l\mu}^T e_{la}(\bar{\mathbf{q}} + \mathbf{Q}) e_{la}^T(\bar{\mathbf{q}} + \mathbf{Q}) e_{l\nu}, \quad (\text{D10})$$

where $e_{la}(\mathbf{q})$ is defined in Eq. (B18). Then comes the moiré potential. The moiré potential usually contains two parts, one is the intralayer part that is mainly due to lattice relaxation, and the other is the interlayer part mainly due to the interlayer commensurate scattering. For simplicity, we retain only the hoppings among nearest \mathbf{Q} vectors (just like the BM model). The intralayer moiré potential can then be written as the $\bar{\mathbf{q}}$ -independent form

$$\delta\mathcal{D}_{\mathbf{Q}l\mu, \mathbf{Q}l\nu}^{\text{intra}} = \sum_{j=1,2,3} \left[B_{l\mu, l\nu}(\mathbf{G}_j^m) \delta_{\mathbf{Q}, \mathbf{Q}' + \mathbf{G}_j^m} + B_{l\mu, l\nu}^*(\mathbf{G}_j^m) \delta_{\mathbf{Q}, \mathbf{Q}' - \mathbf{G}_j^m} \right], \quad (\text{D11})$$

where $\mathbf{G}_1^m = 4\pi/(\sqrt{3}L_\theta)(1/2, -\sqrt{3}/2)$, $\mathbf{G}_2^m = C_{3z}\mathbf{G}_1^m$, $\mathbf{G}_3^m = C_{3z}^{-1}\mathbf{G}_1^m$, L_θ is the moiré supercell length. The B matrix with argument \mathbf{G}_1^m is found to be

$$B_{1,1}(\mathbf{G}_1^m) = \begin{pmatrix} 256.20 - 3.09i & -161.46 - 4.68i \\ -161.46 - 4.68i & -292.64 - 2.84i \end{pmatrix}, \quad (\text{D12})$$

for 2.65° bilayer hBN. The numbers here (and below) are in the unit of THz². The interlayer part is found to be much smaller than the intralayer part, which reads (\bar{l} denotes another layer of l)

$$\delta\mathcal{D}_{\mathbf{Q}l\mu, \mathbf{Q}'\bar{l}\nu}^{\text{inter}} = B_{l\mu, \bar{l}\nu}(\mathbf{0}) \delta_{\mathbf{Q}, \mathbf{Q}'} + \sum_{j=1,2,3} \left[B_{l\mu, \bar{l}\nu}(\mathbf{G}_j^m) \delta_{\mathbf{Q}, \mathbf{Q}' + \mathbf{G}_j^m} + B_{l\mu, \bar{l}\nu}^*(\mathbf{G}_j^m) \delta_{\mathbf{Q}, \mathbf{Q}' - \mathbf{G}_j^m} \right], \quad (\text{D13})$$

with

$$B_{1,2}(\mathbf{0}) = \begin{pmatrix} -7.64 & \\ & -7.64 \end{pmatrix}, \quad B_{1,2}(\mathbf{G}_1^m) = \begin{pmatrix} 9.20 & 6.74 \\ 6.74 & 1.41 \end{pmatrix}. \quad (\text{D14})$$

The other B matrices can be obtained through time reversal \mathcal{T} , C_{3z} and C_{2y} rotations:

$$\begin{aligned} B_{\bar{l}, \bar{l}}(\mathbf{G}_1^m) &= C_{2y} C_{3z} B_{l, l}^*(\mathbf{G}_1^m) C_{3z}^T C_{2y}, \\ B_{l, l'}(\mathbf{G}_2^m) &= C_{3z} B_{l, l'}(\mathbf{G}_1^m) C_{3z}^T, \\ B_{l, l'}(\mathbf{G}_3^m) &= C_{3z}^T B_{l, l'}(\mathbf{G}_1^m) C_{3z}. \end{aligned} \quad (\text{D15})$$

By viewing phonon fields as continuum plane waves with layer and sublattice index, the total dynamical matrix can be written in a more compact form which resembles the BM Hamiltonian,

$$D(-i\nabla, \mathbf{r}) = \begin{pmatrix} D_1^0(-i\nabla) + \delta\mathcal{D}_{1,1}^{\text{intra}}(\mathbf{r}) & \delta\mathcal{D}_{1,2}^{\text{inter}}(\mathbf{r}) \\ \delta\mathcal{D}_{2,1}^{\text{inter}}(\mathbf{r}) & D_2^0(-i\nabla) + \delta\mathcal{D}_{2,2}^{\text{intra}}(\mathbf{r}) \end{pmatrix}, \quad (\text{D16})$$

where $D_l^0(-i\nabla)$ takes the iLO/iLO frequencies, which is diagonal about \mathbf{Q} with matrix element Eq. (D10), and

$$\begin{aligned} \delta\mathcal{D}_{l,l}^{\text{intra}}(\mathbf{r}) &= \sum_{j=1,2,3} B_{l,l}(\mathbf{G}_j^m) e^{i\mathbf{G}_j^m \cdot \mathbf{r}} + h.c., \\ \delta\mathcal{D}_{l,\bar{l}}^{\text{inter}}(\mathbf{r}) &= \frac{1}{2} B_{lA, \bar{l}A'}(\mathbf{0}) + \sum_{j=1,2,3} B_{l,\bar{l}}(\mathbf{G}_j^m) e^{i\mathbf{G}_j^m \cdot \mathbf{r}} + h.c.. \end{aligned} \quad (\text{D17})$$

3. The continuum model for moiré PhP

The continuum model for moiré PhP is easily obtained through the moiré phonon model introduced in the last subsection. First we notice that in moiré systems, the continuum version of displacement field $\mathbf{u}_{l\alpha}$ can be written as

$$\mathbf{u}_{l\alpha}(\mathbf{r}, t) = \sum_{\mathbf{Q}} \mathbf{u}_{l\alpha, \bar{\mathbf{q}}+\mathbf{Q}}(\mathbf{r}, t), \quad (\text{D18})$$

where $\mathbf{u}_{l\alpha, \bar{\mathbf{q}}+\mathbf{Q}} \propto e^{i(\bar{\mathbf{q}}+\mathbf{Q})\cdot\mathbf{r}}$ is the \mathbf{Q} -th Fourier component of $\mathbf{u}_{l\alpha}$ in the layer l . Like Eq. (B22), we define a series of continuum field, characterized by the wave vector \mathbf{Q} , at the layer l ,

$$\mathbf{W}_{\bar{\mathbf{q}}+\mathbf{Q}, l}(\mathbf{r}, t) = \frac{1}{\sqrt{\Omega_0}} \sqrt{\frac{M_N M_B}{M_N + M_B}} [\mathbf{u}_{lN, \bar{\mathbf{q}}+\mathbf{Q}}(\mathbf{r}, t) - \mathbf{u}_{lB, \bar{\mathbf{q}}+\mathbf{Q}}(\mathbf{r}, t)] = \mathbf{W}_{\bar{\mathbf{q}}+\mathbf{Q}, l} e^{i(\bar{\mathbf{q}}+\mathbf{Q})\cdot\mathbf{r}}. \quad (\text{D19})$$

The complete continuum \mathbf{W} field consists of components with different wave vectors and layers $\mathbf{W}(\mathbf{r}, t) = \sum_{\mathbf{Q}l} \mathbf{W}_{\bar{\mathbf{q}}+\mathbf{Q}, l} e^{i(\bar{\mathbf{q}}+\mathbf{Q})\cdot\mathbf{r}}$, so does the continuum \mathbf{P} field

$$\mathbf{P}(\mathbf{r}, t) = \frac{1}{\Omega_0} \sum_{l\alpha} Z_\alpha e \mathbf{u}_{l\alpha}(\mathbf{r}, t) = \gamma \sum_{\mathbf{Q}l} \mathbf{W}_{\bar{\mathbf{q}}+\mathbf{Q}, l} e^{i(\bar{\mathbf{q}}+\mathbf{Q})\cdot\mathbf{r}} = \sum_{\mathbf{Q}} \mathbf{P}_{\bar{\mathbf{q}}+\mathbf{Q}} e^{i(\bar{\mathbf{q}}+\mathbf{Q})\cdot\mathbf{r}}, \quad (\text{D20})$$

where $\gamma = Z_N e (M_N^{-1} + M_B^{-1})^{1/2} \Omega_0^{-1/2}$ takes the same form as monolayer case Eq. (B27). We see the \mathbf{Q} -component of \mathbf{P} and \mathbf{W} are related simply through

$$\mathbf{P}_{\bar{\mathbf{q}}+\mathbf{Q}} = \gamma (\mathbf{W}_{\bar{\mathbf{q}}+\mathbf{Q}, 1} + \mathbf{W}_{\bar{\mathbf{q}}+\mathbf{Q}, 2}). \quad (\text{D21})$$

With the multi-component electric field $\mathbf{E}(\mathbf{r}, t) = \sum_{\mathbf{Q}} \mathbf{E}_{\bar{\mathbf{q}}+\mathbf{Q}} e^{i(\bar{\mathbf{q}}+\mathbf{Q})\cdot\mathbf{r}}$, the equation of motion for \mathbf{W} becomes a hybrid matrix equation

$$\ddot{\mathbf{W}}_{\bar{\mathbf{q}}+\mathbf{Q}, l\mu} = - \sum_{\mathbf{Q}'l'\nu} \mathcal{D}_{\mathbf{Q}l\mu, \mathbf{Q}'l'\nu}(\bar{\mathbf{q}}) \mathbf{W}_{\bar{\mathbf{q}}+\mathbf{Q}', l'\nu} + \gamma \mathbf{E}_{\bar{\mathbf{q}}+\mathbf{Q}, \mu}, \quad (\text{D22})$$

where $\mathcal{D}(\bar{\mathbf{q}})$ is just the dynamical matrix in the continuum model of moiré phonons, under basis Eq. (D8), i.e., Eqs. (D10), (D11), and (D13). For further simplification we can even neglect the $\bar{\mathbf{q}}$ -dependence of the force field, i.e., $\mathcal{D}(\bar{\mathbf{q}}) = \mathcal{D}(\mathbf{0})$. If so, the $\bar{\mathbf{q}}$ -dependence of PhP only comes from the EM waves, i.e., through the introduction of parameters $\lambda_{\bar{\mathbf{q}}}^2 = (\bar{\mathbf{q}} + \mathbf{Q})^2 - \omega^2/c^2$. For a more accurate calculation, we should retain $\bar{\mathbf{q}}$ -dependence of the force field.

The following discussion is parallel to the toy model. Suppose $\mathbf{w}_{\bar{\mathbf{q}}b}$ diagonalizes $\mathcal{D}(\bar{\mathbf{q}})$, and the plane waves are expanded using normal modes as $\mathbf{W}_{\bar{\mathbf{q}}+\mathbf{Q}, l\mu} = \sum_b U_{\mathbf{Q}l\mu, b}(\bar{\mathbf{q}}) w_{\bar{\mathbf{q}}b}$ [notice that $\mathcal{D}(\bar{\mathbf{q}})U(\bar{\mathbf{q}}) = U(\bar{\mathbf{q}})\text{Diag}(\omega_{\bar{\mathbf{q}}b}^2)$]. Then if the system oscillates under the electric field with frequency ω we can solve

$$w_{\bar{\mathbf{q}}b} = \frac{\gamma}{\omega_{\bar{\mathbf{q}}b}^2 - \omega^2} \sum_{\mathbf{Q}l\mu} E_{\bar{\mathbf{q}}+\mathbf{Q}, \mu} U_{\mathbf{Q}l\mu, b}^*(\bar{\mathbf{q}}). \quad (\text{D23})$$

So the polarization

$$\mathbf{P}_{\bar{\mathbf{q}}+\mathbf{Q}, \mu} = \gamma \sum_l \mathbf{W}_{\bar{\mathbf{q}}+\mathbf{Q}, l\mu} = \gamma \sum_{lb} w_{\bar{\mathbf{q}}b} U_{\mathbf{Q}l\mu, b}(\bar{\mathbf{q}}) = \sum_{\mathbf{Q}'l'\nu} \sum_{bll'} \frac{\gamma^2}{\omega_{\bar{\mathbf{q}}b}^2 - \omega^2} U_{\mathbf{Q}l\mu, b}(\bar{\mathbf{q}}) U_{\mathbf{Q}'l'\nu, b}^*(\bar{\mathbf{q}}) E_{\bar{\mathbf{q}}+\mathbf{Q}', \nu}, \quad (\text{D24})$$

from which we read

$$\varepsilon_0 \Pi_{\mu\nu}^{\mathbf{Q}\mathbf{Q}'}(\bar{\mathbf{q}}) = \gamma^2 \sum_{bll'} \frac{U_{\mathbf{Q}l\mu, b}(\bar{\mathbf{q}}) U_{\mathbf{Q}'l'\nu, b}^*(\bar{\mathbf{q}})}{\omega_{\bar{\mathbf{q}}b}^2 - \omega^2}. \quad (\text{D25})$$

We have listed some results in Fig. 7 calculated using the present continuum model for 2.65° twisted bilayer hBN. Both the moiré PhP bands and local susceptibility are well accurately recovered [compared to those shown in the main text obtained through the lattice model]. We have tried artificially turned off the moiré potential by setting Eq. (D17) to be zero. In such case the system consists of two decoupled bilayers, where all moiré physics disappear: the multiple flat moiré PhPs are missing, and the local susceptibility shows no signal difference between AA- and AB-stacking points.

The continuum model can be conveniently used to study systems with smaller twisting angles. Here our continuum model has a intralayer moiré potential that is much stronger than the interlayer part. We may expect the strong twisting-dependence of the model parameters, since the correlation becomes dominant at smaller angles. One must be careful to tune the intralayer parameters Eq. (D12) when using it to study systems with much larger supercells. We will leave the detailed determination of this model in the future.

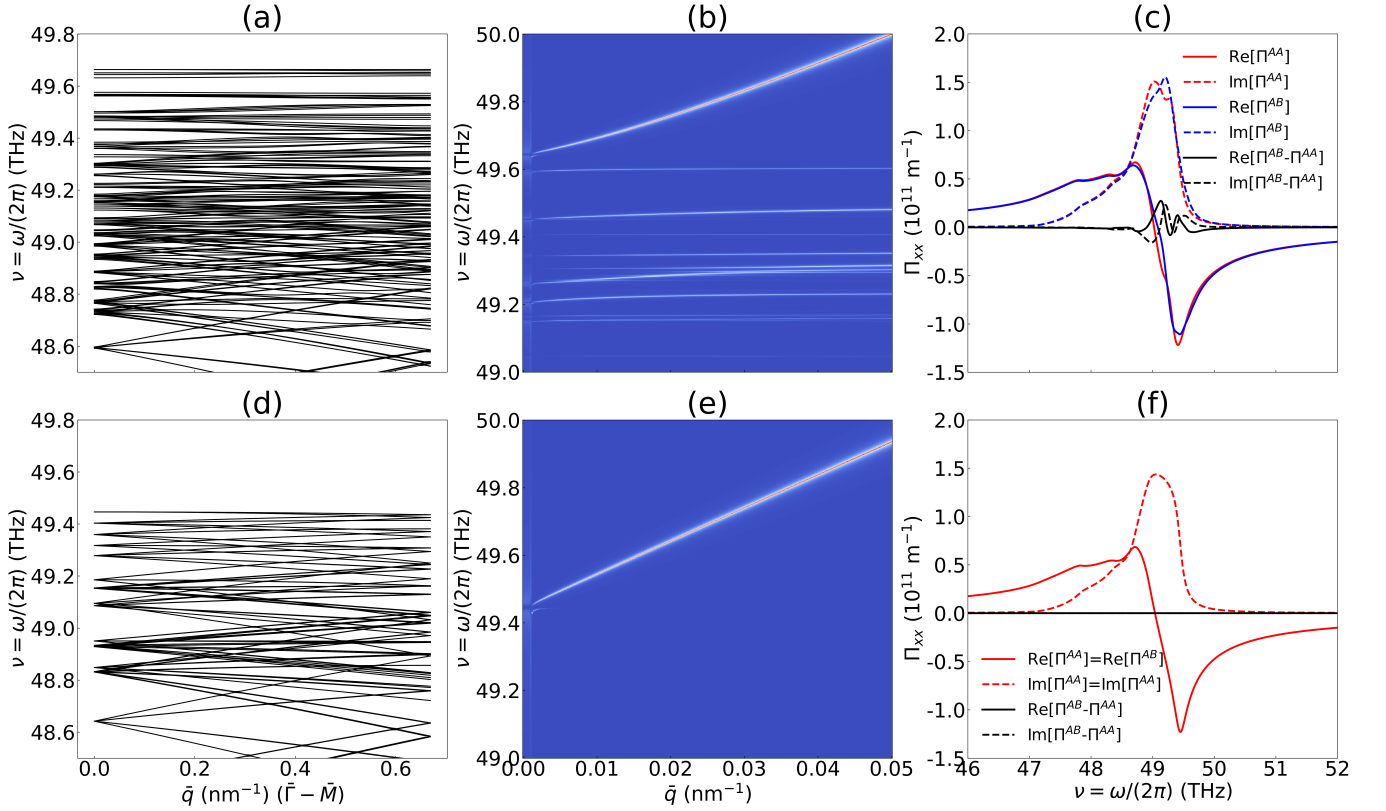


FIG. 7. The phonon bands [(a), (d)], PhP bands [(b), (e)], and local susceptibility $\Pi_{xx}(\mathbf{r}, \mathbf{r}, \omega)$ [(c), (f)], calculated using the continuum model constructed in Secs. D 2 and D 3. (a), (b), (c) are the results of 2.65° twisted bilayer hBN, while in (d), (e), (f) we have turned off the moiré potential, i.e., we set $\delta\mathcal{D}^{\text{intra}} = \delta\mathcal{D}^{\text{inter}} = 0$. All calculations only use 61 \mathbf{Q} vectors. In (b), (e) we use the linewidth $\delta/(2\pi) = 0.001$ THz. In (c), (f) we use $\delta/(2\pi) = 0.15$ THz.

Appendix E: More details about the moiré response function

1. Derivation in quantum case

The response function used in the main text is also valid if phonons are treated quantum mechanically. We re-derived it using the linear response theory. The displacement operator is

$$\hat{\mathbf{u}}(\mathbf{r}_{I\alpha}) = \sum_{\bar{\mathbf{q}}b} \sqrt{\frac{\hbar}{2M_\alpha\omega_{\bar{\mathbf{q}}b}N_m}} \mathbf{e}_{i\alpha,b}(\bar{\mathbf{q}}) e^{i\bar{\mathbf{q}}\cdot\mathbf{r}_{I\alpha}} (\hat{a}_{\bar{\mathbf{q}}b} + \hat{a}_{-\bar{\mathbf{q}}b}^\dagger), \quad (\text{E1})$$

where $\hat{a}_{\bar{\mathbf{q}}b}$, $\hat{a}_{\bar{\mathbf{q}}b}^\dagger$ are operators of phonon mode $\bar{\mathbf{q}}, b$, satisfying $[\hat{a}_{\bar{\mathbf{q}}b}, \hat{a}_{\bar{\mathbf{q}}'b'}^\dagger] = \delta_{\bar{\mathbf{q}}\bar{\mathbf{q}}'}\delta_{bb'}$. The polarization operator, defined like Eq. (C4), is expanded in Fourier space

$$\hat{\mathbf{P}}(\mathbf{r}) = \sum_{\bar{\mathbf{q}}\mathbf{Q}} e^{i(\bar{\mathbf{q}}+\mathbf{Q})\cdot\mathbf{r}} \hat{\mathbf{P}}_{\bar{\mathbf{q}}+\mathbf{Q}}, \quad (\text{E2})$$

where $\hat{\mathbf{P}}_{\bar{\mathbf{q}}+\mathbf{Q}}$ can be calculated similar to Eq. (C12),

$$\hat{\mathbf{P}}_{\bar{\mathbf{q}}+\mathbf{Q}} = \frac{e}{\Omega_m} \sum_b \mathbf{S}_{\mathbf{Q}b}(\bar{\mathbf{q}}) \sqrt{\frac{\hbar}{2\omega_{\bar{\mathbf{q}}b}N_m}} (\hat{a}_{\bar{\mathbf{q}}b} + \hat{a}_{-\bar{\mathbf{q}}b}^\dagger), \quad (\text{E3})$$

with the form factor $\mathbf{S}_{\mathbf{Q}b}(\bar{\mathbf{q}})$ defined in Eq. (C10).

With field $\mathbf{E}_t(\mathbf{r}, t) = \sum_{\mathbf{Q}} \mathbf{E}_{\bar{\mathbf{q}}+\mathbf{Q},t}(\omega) e^{i(\bar{\mathbf{q}}+\mathbf{Q})\cdot\mathbf{r} - i\omega t}$, the total Hamiltonian reads

$$\hat{H} = \hat{H}_0 + \hat{H}_{\text{res}}, \quad (\text{E4})$$

where $\hat{H}_0 = \sum_{\bar{q}b} \hbar\omega_{\bar{q}b} \hat{a}_{\bar{q}b}^\dagger \hat{a}_{\bar{q}b}$, and $(\Omega_{\text{tot}} = N_m \Omega_m)$

$$\hat{H}_{\text{res}} = - \int d\mathbf{r} \hat{\mathbf{P}}(\mathbf{r}) \cdot \mathbf{E}_t(\mathbf{r}, t) = -\Omega_{\text{tot}} \sum_{\mathbf{Q}'} \hat{\mathbf{P}}_{-\bar{q}-\mathbf{Q}'} \cdot \mathbf{E}_{\bar{q}+\mathbf{Q}', t}(\omega) e^{-i\omega t}. \quad (\text{E5})$$

Treating \hat{H}_{res} as external coupling, then the expectation $P_{\bar{q}+\mathbf{Q}}(t) = \langle \hat{\mathbf{P}}_{\bar{q}+\mathbf{Q}} \rangle(t) - \langle \hat{\mathbf{P}}_{\bar{q}+\mathbf{Q}} \rangle_0$ reads from the Kubo formula as

$$P_{\bar{q}+\mathbf{Q}, \mu}(t) = \sum_{\mathbf{Q}'\nu} \varepsilon_0 \Pi_{\mu\nu}^{\mathbf{Q}\mathbf{Q}'}(\bar{\mathbf{q}}, \omega) E_{\bar{q}+\mathbf{Q}', \nu}(\omega) e^{-i\omega t}, \quad (\text{E6})$$

where

$$\Pi^{\mathbf{Q}\mathbf{Q}'}(\bar{\mathbf{q}}, \omega) = -\frac{N_m \Omega_m}{\varepsilon_0 \hbar} \sum_{mn} \frac{[\hat{\mathbf{P}}_{\bar{q}+\mathbf{Q}}]_{mn} [\hat{\mathbf{P}}_{-\bar{q}-\mathbf{Q}'}^T]_{nm}}{\omega + (E_m - E_n)/\hbar + i0^+} \frac{1}{\mathcal{Z}_0} (e^{-\beta E_m} - e^{-\beta E_n}). \quad (\text{E7})$$

Here $\beta = 1/(k_B T)$, $\mathcal{Z}_0 = \text{Tr}(e^{-\beta \hat{H}_0})$ is the partition function, and $[\hat{O}]_{mn} = \langle m | \hat{O} | n \rangle$ is the matrix element in the phonon Fock basis $|m\rangle, |n\rangle$ with energies E_m, E_n , respectively. Since $\hat{\mathbf{P}}_{\bar{q}+\mathbf{Q}} \propto \hat{a}_{\bar{q}b} + \hat{a}_{-\bar{q}b}^\dagger$, in the summation only the following terms survive

$$|m\rangle = N_{n, \bar{q}b}^{-1/2} \hat{a}_{\bar{q}b} |n\rangle \quad \text{or} \quad |n\rangle = N_{m, -\bar{q}b}^{-1/2} \hat{a}_{-\bar{q}b} |m\rangle, \quad (\text{E8})$$

where $N_{n, \bar{q}b}$ is the multiplicity of the \bar{q}, b phonon in state $|n\rangle$. The two cases give $E_n - E_m = \hbar\omega_{\bar{q}b}$ and $E_m - E_n = \hbar\omega_{-\bar{q}b}$, respectively. Using Eq. (E16) and the bosonic statistics

$$\mathcal{Z}_0^{-1} \sum_n e^{-\beta E_n} N_{n, \bar{q}b} = (e^{\beta \hbar\omega_{\bar{q}b}} - 1)^{-1}, \quad (\text{E9})$$

the calculation follows

$$\begin{aligned} \Pi^{\mathbf{Q}\mathbf{Q}'}(\bar{\mathbf{q}}, \omega) &= -\frac{e^2}{\varepsilon_0 \Omega_m} \sum_{mn} \sum_{bb'} \frac{\mathbf{S}_{Qb}(\bar{\mathbf{q}}) \mathbf{S}_{Q'b'}^\dagger(\bar{\mathbf{q}})}{\sqrt{2\omega_{\bar{q}b}} \sqrt{2\omega_{\bar{q}b'}}} \frac{[\hat{a}_{\bar{q}b} + \hat{a}_{-\bar{q}b}^\dagger]_{mn} [\hat{a}_{-\bar{q}b'} + \hat{a}_{\bar{q}b'}^\dagger]_{nm}}{\omega + (E_m - E_n)/\hbar + i0^+} \frac{1}{\mathcal{Z}_0} (e^{-\beta E_m} - e^{-\beta E_n}) \\ &= \frac{e^2}{\varepsilon_0 \Omega_m} \sum_b \frac{\mathbf{S}_{Qb}(\bar{\mathbf{q}}) \mathbf{S}_{Q'b}^\dagger(\bar{\mathbf{q}})}{2\omega_{\bar{q}b}} \left(\frac{1}{\omega - \omega_{\bar{q}b} + i0^+} - \frac{1}{\omega + \omega_{\bar{q}b} + i0^+} \right) (1 - e^{\beta \hbar\omega_{\bar{q}b}}) \sum_n \frac{N_{n, \bar{q}b}}{\mathcal{Z}_0} e^{-\beta E_n} \\ &= \frac{e^2}{\varepsilon_0 \Omega_m} \sum_b \frac{\mathbf{S}_{Qb}(\bar{\mathbf{q}}) \mathbf{S}_{Q'b}^\dagger(\bar{\mathbf{q}})}{\omega_{\bar{q}b}^2 - \omega^2 - i\omega 0^+}. \end{aligned} \quad (\text{E10})$$

In Ref. [55] the authors reach the (moiré-less version of) above formula in the $T = 0$ limit. The derivation here indicates that the expression actually is *temperature-independent*.

2. Non-locality and inhomogeneity

The moiré polar system realizes the spatially non-local response, in the sense that

$$\mathbf{P}(\mathbf{r}, t) = \int d\mathbf{r}' dt' \varepsilon_0 \mathbf{\Pi}(\mathbf{r}, \mathbf{r}', t - t') \mathbf{E}(\mathbf{r}', t'). \quad (\text{E11})$$

Here the moiré response function, defined as

$$\mathbf{\Pi}(\mathbf{r}, \mathbf{r}', t) = \frac{1}{2\pi \Omega_{\text{tot}}} \int d\omega \sum_{\bar{\mathbf{q}}\mathbf{Q}\mathbf{Q}'} \mathbf{\Pi}^{\mathbf{Q}\mathbf{Q}'}(\bar{\mathbf{q}}, \omega) e^{i(\bar{\mathbf{q}}+\mathbf{Q})\cdot\mathbf{r} - i(\bar{\mathbf{q}}+\mathbf{Q}')\cdot\mathbf{r}'} e^{-i\omega t}, \quad (\text{E12})$$

is translation invariant only with moiré period

$$\mathbf{\Pi}(\mathbf{r}, \mathbf{r}', t) = \mathbf{\Pi}(\mathbf{r} + \mathbf{L}_I, \mathbf{r}' + \mathbf{L}_I, t). \quad (\text{E13})$$

For a general vector \mathbf{a} that is incommensurate with moiré lattice, the non-locality indicates $\mathbf{\Pi}(\mathbf{r}, \mathbf{r}', t) \neq \mathbf{\Pi}(\mathbf{r} + \mathbf{a}, \mathbf{r}' + \mathbf{a}, t)$, which is different from the moiré-less case. By transforming the above formula into the frequency space, and setting $\mathbf{r}' = \mathbf{r}$, we obtain the local susceptibility in the main text.

3. Symmetry properties

For simplicity let's consider the non-degenerate case, i.e., $\omega_{\bar{q}b} \neq \omega_{\bar{q}b'}$ when $b \neq b'$. The time reversal requires

$$\omega_{-\bar{q},b} = \omega_{\bar{q}b}, \quad \mathbf{e}_{i\alpha,b}(-\bar{\mathbf{q}}) = \mathbf{e}_{i\alpha,b}^*(\bar{\mathbf{q}}), \quad (\text{E14})$$

while the point group rotation g (of the system) requires

$$\omega_{g\bar{q},b} = \omega_{\bar{q}b}, \quad g\mathbf{e}_{g^{-1}(i\alpha),b}(\bar{\mathbf{q}}) = \mathbf{e}_{i\alpha,b}(g\bar{\mathbf{q}}). \quad (\text{E15})$$

These give the following constraints on the S matrix

$$\mathbf{S}_{Qb}(\bar{\mathbf{q}}) = [\mathbf{S}_{-Qb}(-\bar{\mathbf{q}})]^*, \quad (\text{E16})$$

$$\mathbf{S}_{Qb}(\bar{\mathbf{q}}) = g^{-1}\mathbf{S}_{gQ,b}(g\bar{\mathbf{q}}). \quad (\text{E17})$$

As a result, the response function satisfies

$$\Pi^{QQ'}(\bar{\mathbf{q}}, \omega) = [\Pi^{-Q,-Q'}(-\bar{\mathbf{q}}, -\omega)]^*, \quad (\text{E18})$$

$$\Pi^{QQ'}(\bar{\mathbf{q}}, \omega) = g^{-1}\Pi^{gQ,gQ'}(g\bar{\mathbf{q}}, \omega)g. \quad (\text{E19})$$

The last identity also holds if there exists degeneracy [in this case we have $g\mathbf{S}_{Qb_j}(\bar{\mathbf{q}}) = \sum_{j'} \mathbf{S}_{gQ,b_{j'}}(g\bar{\mathbf{q}})U_{j'j}^g(\bar{\mathbf{q}})$ instead, where $b_{j(j')}$ takes from the degenerate subspace, and the matrix $U^g(\bar{\mathbf{q}})$ is unitary]. Besides, the form of Eq. (C14) itself has an additional property

$$\Pi^{QQ'}(\bar{\mathbf{q}}, \omega) = [\Pi^{Q'Q}(\bar{\mathbf{q}}, -\omega)]^\dagger. \quad (\text{E20})$$

If $\mathbf{E}(\mathbf{r}, t)$ is an eigen mode, then so is $\mathbf{E}^*(\mathbf{r}, t)$, as told by Eq. (E18). This guarantees that the eigen fields can always taken to be real. On the other hand, Eq. (E19) indicates that the rotated field $g\mathbf{E}(g^{-1}\mathbf{r}, t)$ is also an eigen solution with the same dispersion.

4. Representation in moiré-less basis

Suppose with the moiré potential, the eigen displacement $\mathbf{e}_{i\alpha,b}(\bar{\mathbf{q}})$ (with eigen frequency $\omega_{\bar{q}b}$) is related to the (folded) moiré-less one $\mathbf{e}_{\alpha,la}(\bar{\mathbf{q}} + \mathbf{Q})$ (with frequency $\omega_{\bar{\mathbf{q}}+\mathbf{Q},la}^0$) by Eq. (D5) [35, 36]

$$\mathbf{e}_{i\alpha,b}(\bar{\mathbf{q}}) = \sum_{Qla} \frac{e^{i\mathbf{Q}\cdot(\mathbf{R}_i+\boldsymbol{\tau}_\alpha)}}{\sqrt{N_a}} \mathbf{e}_{\alpha,la}(\bar{\mathbf{q}} + \mathbf{Q})U_{Qla,b}(\bar{\mathbf{q}}). \quad (\text{E21})$$

The matrix U is determined by the moiré potential (dynamical matrix) $D^m(\bar{\mathbf{q}})$, satisfying $U^\dagger U = UU^\dagger = I$ and $U_{-Qla,b}(-\bar{\mathbf{q}}) = U_{Qla,b}^*(\bar{\mathbf{q}})$. Using the identity [36]

$$\frac{1}{N_a} \sum_i e^{i\mathbf{Q}\cdot\mathbf{R}_i} = \delta_{\mathbf{Q}\mathbf{0}}, \quad (\text{E22})$$

the moiré S matrix Eq. (C10) is found related with the moiré-less one Eq. (B9) through

$$\mathbf{S}_{Qb}(\bar{\mathbf{q}}) = \sqrt{N_a} \sum_a \mathbf{S}_{la}(\bar{\mathbf{q}} + \mathbf{Q})U_{Qla,b}(\bar{\mathbf{q}}). \quad (\text{E23})$$

So from Eq. (C14) we get

$$\varepsilon_0 \Pi^{QQ'}(\bar{\mathbf{q}}, \omega) = \frac{e^2}{\Omega_0} \sum_b \sum_{la} \sum_{l'a'} \frac{\mathbf{S}_{la}(\bar{\mathbf{q}} + \mathbf{Q})\mathbf{S}_{l'a'}^\dagger(\bar{\mathbf{q}} + \mathbf{Q}')}{\omega_{\bar{q}b}^2 - \omega^2} U_{Qla,b}(\bar{\mathbf{q}})U_{Q'l'a',b}^*(\bar{\mathbf{q}}), \quad (\text{E24})$$

which is equivalent to Eq. (D25) if one approximates $\mathbf{S}_{la}(\bar{\mathbf{q}} + \mathbf{Q}) \approx \mathbf{S}_{la}(\mathbf{0})$. In the moiré-less case where \mathbf{Q} is a good quantum number, $U_{Qla,b} = \delta_{Qla,b}$, and $\Pi(\omega)$ reduces to the diagonal moiré-less one Eq. (B13) as well. We see the off-diagonal term of $\Pi^{QQ'}$ results from the off-diagonal elements of U , whose strength is proportional to the moiré potential from the perturbation viewpoint ($Qla \neq Q'l'a'$, $\delta\mathcal{D}$ is the moiré potential):

$$U_{Qla,Q'l'a'}(\bar{\mathbf{q}}) \sim \frac{e_{la}^\dagger(\bar{\mathbf{q}} + \mathbf{Q})\delta\mathcal{D}(\bar{\mathbf{q}})e_{l'a'}(\bar{\mathbf{q}} + \mathbf{Q}')}{\omega_{\bar{\mathbf{q}}+\mathbf{Q}',l'a'}^2 - \omega_{\bar{\mathbf{q}}+\mathbf{Q},la}^2}. \quad (\text{E25})$$

Appendix F: Interatomic force constant

We utilize the frozen phonon method to compute the interatomic force constant (FC), which by definition reads

$$\Phi_{i\alpha\mu,j\beta\nu}(\mathbf{r}_{Ii\alpha} - \mathbf{r}_{Jj\beta}) = \frac{\partial^2 U}{\partial u_\mu(\mathbf{r}_{Ii\alpha}) \partial u_\nu(\mathbf{r}_{Jj\beta})}. \quad (\text{F1})$$

The potential energy $U = U_{\text{intra}} + U_{\text{inter}}$, including energy from intralayer and interlayer atoms. Specifically, for hBN, U_{intra} is modeled by the Tersoff potential [46], and U_{inter} is modeled by the registry-dependent interlayer potential [47] tailored for the twisted bilayer hBN [48, 49]. For MoTe₂, we use Stillinger-Weber potential [50] parameterized by Jiang [51] to model the intralayer interactions. For the interlayer interactions, parameters fitted for TMD systems [52, 53] is used.

Before computing FC, the minimization algorithms of conjugate-gradient and *fire* are sequentially preformed to optimize the simulation cell and atomic positions, using large-scale atomic/molecular massively parallel simulator (LAMMPS) [54]. We have intentionally avoided performing the non-analytical correction on the dynamical matrix, because otherwise it results in a double counting of the Coulomb force. We note that different FC computed from different force fields could indeed quantitatively influence the polariton dispersion, since the moiré physics happens always in tiny energy scales. Nevertheless, their qualitative moiré structure should be robust and will not be altered by quantitative differences.
